ΠΑΝΕΠΙΣΤΗΜΙΟ ΙΩΑΝΝΙΝΩΝ
ΣΧΟΛΗ ΘΕΤΙΚΩΝ ΕΠΙΣΤΗΜΩΝ
ΤΜΗΜΑ ΜΑΘΗΜΑΤΙΚΩΝ
ΤΟΜΕΑΣ ΕΦΑΡΜΟΣΜΕΝΩΝ
ΚΑΙ ΥΠΟΛΟΓΙΣΤΙΚΩΝ ΜΑΘΗΜΑΤΙΚΩΝ

ΑΝΑΛΥΤΙΚΕΣ ΚΑΙ ΑΡΙΘΜΗΤΙΚΕΣ ΛΥΣΕΙΣ ΜΗ ΓΡΑΜΜΙΚΩΝ ΕΞΕΛΙΚΤΙΚΩΝ ΜΕΡΙΚΩΝ ΔΙΑΦΟΡΙΚΩΝ ΕΞΙΣΩΣΕΩΝ ΣΤΗ ΡΕΥΣΤΟΔΥΜΑΝΙΚΗ

Αναστάσιος Φελιάς

ΜΕΤΑΠΤΥΧΙΑΚΗ ΔΙΑΤΡΙΒΗ

Ιωάννινα, 2022

UNIVERSITY OF IOANNINA
SCHOOL OF SCIENCES
DEPARTMENT OF MATHEMATICS
SECTION OF APPLIED
AND COMPUTATIONAL MATHEMATICS

ANALYTICAL AND NUMERICAL SOLUTIONS TO NONLINEAR EVOLUTION PARTIAL DIFFERNTIAL EQUATIONS IN FLUID DYNAMICS

Anastasios Felias

MASTER'S THESIS

Ioannina, 2022

Αφιερώνεται στην οικογένειά μου, στον καθηγητή μου κύριο Γεώργιο Παππά, καθώς και σε κάθε συμβουλή και εμπόδιο που συνάντησα κατά τη συγγραφή

Dedicated to my family, to my professor Mr. George Pappas, as well as to any advice and obstable occuring on the writing process

Η παρούσα Μεταπτυχιακή Διατριβή εκπονήθηκε στο πλαίσιο των σπουδών για την απόκτηση του Μεταπτυχιακού Διπλώματος Ειδίκευσης στα Εφαρμοσμένα Μαθηματικά και την Πληροφορική που απονέμει το Τμήμα Μαθηματικών του Πανεπιστημίου Ιωαννίνων.

Εγκρίθηκε την 25/02/2022 από την εξεταστική επιτροπή:

Ονοματεπώνυμο	**Βαθμίδα**
Μιχαήλ Ξένος	Αναπληρωτης Καθηγητής (Επιβλέπων)
Φωτεινή Καρακατσάνη	Επίκουρη Καθηγήτρια
Ευστράτιος Τζιρτζιλάκης	Καθηγητής

ΥΠΕΥΘΥΝΗ ΔΗΛΩΣΗ

"Δηλώνω υπεύθυνα ότι η παρούσα διατριβή εκπονήθηκε κάτω από τους διεθνείς ηθικούς και ακαδημαϊκούς κανόνες δεοντολογίας και προστασίας της πνευματικής ιδιοκτησίας. Σύμφωνα με τους κανόνες αυτούς, δεν έχω προβεί σε ιδιοποίηση ξένου επιστημονικού έργου και έχω πλήρως αναφέρει τις πηγές που χρησιμοποίησα στην εργασία αυτή."

Αναστάσιος Φελιάς

Ευχαριστιες

Η παρούσα διατριβή έχει πραγματοποιηθεί στο Τμήμα Μαθηματικών του Πανεπιστημίου Ιωαννίνων. Με την ολοκλήρωση της παρούσας διατριβής θα ήθελα να ευχαριστήσω κάποιους ανθρώπους, των οποίων η συμβολή ήταν καθοριστική σε αυτή τη μελέτη.

Αρχικά θα ήθελα να ευχαριστήσω τον επιβλέποντα καθηγητή μου κύριο Μιχαήλ Ξένο, για τη βοήθεια, τις πολύτιμες συμβουλές, τον χρόνο, την υποστήριξη, την καθοδήγηση, την ενθάρρυνση και αμέριστη συμπαράσταση που μου προσέφερε κατά τη διάρκεια της εκπόνησης της εργασίας. Ελπίζω ότι και ο ίδιος γνωρίζει ότι τον εκτιμώ όχι μόνο ως καθηγητή, αλλά και ως άνθρωπο.

Ιδιαίτερα θέλω να ευχαριστήσω και τα άλλα δύο μέλη της τριμελούς εξεταστικής επιτροπής, κυρία Φωτεινή Καρακατσάνη και κύριο Ευστράτιο Τζιρτζιλάκη, για το ενδιαφέρον που έδειξαν, τον χρόνο που διέθεσαν αλλά και για τις εύστοχες παρατηρήσεις και υποδείξεις τους στην διατριβή αυτή με σκοπό την βελτίωση της.

Ακόμη θα ήθελα να ευχαριστήσω όλους του διδάσκοντες του Τμήματος Μαθηματικών για τις γνώσεις που μου προσέφεραν σε Προπτυχιακό και Μεταπτυχιακό επίπεδο και τη συνεργασία που είχαμε όλα αυτά τα χρόνια.

Θα ήθελα, επιπλέον, να πω ένα ευχαριστώ στον κύριο Γεώργιο Παππά, ο οποίος μου έχει εκμαιεύσει το πάθος μου προς τα Μαθηματικά από τα μαθητικά μου χρόνια.

Το πιο μεγάλο ευχαριστώ ανήκει δικαιωματικά στην οικογένεια μου, που με στήριξε με όλους τους δυνατούς τρόπους ώστε να ολοκληρώσω τις μεταπτυχιακές μου σπουδές και θα συνεχίσει να με στηρίζει σε όλα τα μελλοντικά μου σχέδια.

Ιωάννινα 2022,
Αναστάσιος Φελιάς

Acknowledgements

This dissertation has been compiled at the Department of Mathematics of the University of Ioannina. With the completion of this dissertation, I would like to thank some people, whose contribution was decisive in this study.

Initially, I would like to thank my supervisor, Mr. Michael Xenos, for his help, valuable advice, time, support, guidance and the encouragement that he offered me during my study. I hope he knows that I appreciate him not only as a professor, but as a person as well.

In particular, I would like to thank the other two members of the three-member examination committee, Mrs. Foteini Karakatsani and Mr. Efstratios Tzirtzilakis, for the interest they showed, the time they spent, but also for their precise corrections and suggestions in this dissertation for its improvement.

I would also like to thank all the professors of the Department of Mathematics for the knowledge they have offered me at the undergraduate and postgraduate level and the cooperation we have had over the years.

Furthermore, I would like to thank Mr. George Pappas, who has educed me my passion towards Mathematics since my Highschool years.

The biggest thank rightfully goes to my family, who supported in every possible way to complete my graduate studies and will continue to support me in all my future plans.

Ioannina 2022,
Anastasios Felias

Περιληψη

Η μελέτη αναλυτικών λύσεων μη γραμμικών εξισώσεων συνιστά ένα ενεργό πεδίο έρευνας τόσο των θεωρητικών όσο και των εφαρμοσμένων μαθηματικών. Πολλά από τα πιο ενδιαφέροντα χαρακτηριστικά των φυσικών συστημάτων κρύβονται στη μη γραμμική συμπεριφορά τους και μπορούν να μελετηθούν μόνο με κατάλληλες μεθόδους, σχεδιασμένες για την αντιμετώπιση μη γραμμικών προβλημάτων. Επομένως, η αναζήτηση κατάλληλων μεθόδων επίλυσης, αναλυτικών, προσεγγιστικών ή αριθμητικών, είναι ένα ενεργό ερευνητικό πεδίο στον κλάδο των εφαρμοσμένων και υπολογιστικών μαθηματικών.

Σύνθετα φαινόμενα σε αξιοσημείωτα επιστημονικά πεδία, όπως είναι η ρευστοδυναμική, η καρδιακή αιμοδυναμική και η νευρωνική δυναμική, μπορούν να μοντελοποιηθούν μαθηματικά με την βοήθεια των εξισώσεων Womersley, Korteweg-de Vries-Burgers (KdV-B), Benjamin–Bona–Mahony (BBM), Boussinesq, Burgers, Burgers–Huxley (BH), Camassa–Holm (CH), Degasperis–Procesi (DP), Davey–Stewartson (DS) και Kadomtsev–Petviashvili (KP).

Εντοπισμένες κυματικές λύσεις, συχνά αναφερόμενες ως μονήρη κύματα ή παλμοί, αποτελούνε κυρίαρχο αντικείμενο μελέτης στη θεωρία των μη γραμμικών ολοκληρώσιμων εξισώσεων και συνιστούν σημαντικές κλάσεις λύσεων των προαναφερθέντων εξισώσεων. Σε αυτή την εργασία αναζητούνται αναλυτικές λύσεις για καθεμία από τις προαναφερθείσες εξισώσεις μέσω οδευόντων κυμάτων, περιοδικών κυμάτων και μετασχηματισμών ομοιότητας, καθώς και μέσω των μεθόδων υπερβολικής εφαπτομένης και παραγοντοποίησης. Μέσω της πρώτης, παρουσιάζονται αναλυτικές λύσεις και για τις n-διάστατες εξισώσεις KdV-B και μικτής (compound) KdV-B. Περιγράφεται ο μετασχηματισμός Cole-Hopf, μετατρέποντας την ιξωδική εξίσωση Burgers στην γραμμική εξίσωση μεταφοράς θερμότητας.

Αναλύονται κυματικές αλληλεπιδράσεις μέσω των εξισώσεων BBM, CH και DP. Παράγονται πολυ-κρουστικές λύσεις της ιξωδικής εξίσωσης Burgers και παρουσιάζεται η σύντηξη αυτών σε ένα κρουστικό κύμα. Γραμμικά σολιτόνια λαμβάνονται για την εξίσωση KP. Μελετάται επίσης η εξίσωση Davey–Stewartson

(DS), με εφαρμογές στη ρευστοδυναμική.

Μελετάται ο χώρος φάσεων των εξισώσεων CH, DP και KdV-B. Παρουσιάζεται ο φορμαλισμός της ασθενούς λύσης για τις εξισώσεις CH, DP και την ανιξωδική εξίσωση του Burgers. Επιπλέον, η συνθήκη Rankine-Hugoniot συζητείται στα πλαίσια της μεθόδου των χαρακτηριστικών. Πραγματοποιείται ποιοτική ανάλυση για την ανιξωδική εξίσωση του Burgers και γενικότερα για τις διατηρητικές μορφές. Προσεγγιστικές αναλυτικές λύσεις λαμβάνονται μέσω μεθόδων ομοτοπικής ανάλυσης. Οι αριθμητικές λύσεις προέρχονται μέσω φασματικής ανάλυσης και εξελίσσονται στο χρόνο, χρησιμοποιώντας την άμεση μέθοδο Runge-Kutta 4ης τάξης.

Η εύρεση αναλυτικών λύσεων στα προαναφερθέντα μαθηματικά μοντέλα, είναι μια διαδικασία υψίστης σημασίας. Τέτοιες λύσεις χρησιμοποιούνται ευρέως ως σημεία αναφοράς για αριθμητικές μεθόδους επίλυσης, συμβάλουν σημαντικά στην ανάλυση ευστάθειας, καθώς και ενισχύουν την αντίληψη γύρω από αυτά τα, συνήθως περίπλοκα, μοντέλα. Τα αποτελέσματα και οι εικόνες που παρατίθενται, προέκυψαν σε συνδυασμό και με την χρήση των υπολογιστικών προγραμμάτων MATLAB και WOLFRAM MATHEMATICA.

Abstract

The study of exact solutions to nonlinear equations is an active field of both, pure and applied mathematics. Plenty of the most interesting features of physical systems are hidden in their nonlinear behavior and can only be studied with appropriate methods designed to tackle nonlinearity. Therefore, seeking for suitable solving methods, exact, semi-exact or numerical, is an active task in branches of applied and computational mathematics.

Complex phenomena in notable scientific fields, especially in fluid dynamics, cardiac hemodynamics and neuronal dynamics, can be efficiently mathematically modeled in terms of the Womersley, Korteweg–de Vries–Burgers (KdV–B), Benjamin–Bona–Mahony (BBM), Boussinesq, Burgers, Burgers–Huxley (BH), Camassa–Holm (CH), Degasperis–Procesi (DP), Davey–Stewartson (DS) and Kadomtsev–Petviashvili (KP) equations.

Localized wave solutions, often referred to as solitary waves or pulses, being traditionally a key object of study in the theory of nonlinear integrable equations, are important classes of solutions to the aforementioned equations. Exact solutions are sought for each of the aforementioned equations, by means of traveling wave, periodic wave and similarity transforms, as well as by implementing the hyperbolic tangent and factorization methods. Through the former, analytical solutions are also presented for both the n-dimensional KdV–B and compound KdV–B equations. The Cole–Hopf Transform is described, converting the viscous Burgers equation to the linear Heat transport equation.

Pulse interactions are discussed for the BBM, CH and DP equations. Multi-shock solutions of the viscous Burgers equation are produced, and their fusion into a sole shock wave is presented. Line solitons are obtained for the KP equation. The Davey–Stewartson (DS) equation is also studied, emphasizing to fluid dynamics applications.

Phase plane trajectories are obtained for the CH, DP and KdV–B equations. Weak solution formulation is presented for the CH, DP and inviscid

Burgers equations. Additionally, the Rankine–Hugoniot condition is discussed in the implementation of the method of characteristics. Qualitative analysis is performed for the inviscid Burgers equation, and conservative forms in general. Semi-exact solutions are obtained through a homotopy analysis approach. Numerical solutions are derived by means of spectral Fourier analysis and are evolved in time, using the 4th order explicit Runge–Kutta method.

The derivation of analytical solutions to the aforementioned mathematical models, is a process of high significance. Such solutions are used to benchmark numerical solvers, perform stability analysis and grasp a better understanding of the studied models. The demonstrated results and images resulted by also utilizing the computational softwares of MATLAB and WOLFRAM MATHEMATICA.

Contents

CHAPTER 1

Introduction

Nonlinear evolution partial differential equations connect spatial and time derivatives, in a nonlinear fashion. Complex phenomena in fluid dynamics, cardiac hemodynamics and neuronal dynamics, can be efficiently modeled in terms of evolution equations. The nonlinearity, governing such phenomena, leads to both an unpredictable and a counter-intuitive behavior. The absense of a unified theory to tackle nonlinearity, demands utilizing different techniques for different problems. A mixture of analytical, semi-analytical and numerical approaches is implemented. Completely integrable models have been excessively studied, with the focus shifted towards nonintegrable models [3, 1, 38].

Deriving analytical solutions to nonlinear evolution, not in generally integrable, mathematical models, provides with a benchmark to numerical solvers, a reliable tool for stability analysis, and a deeper sense of the mechanism of the studied models. Several advancements have been implemented along this line. A notable few are the traveling wave solution approach [99], the derivation of self-similar solutions [3], the Tanh method [65, 99] and the factorization method [27].

Recent developments to cardiac hemodynamics can be explained through models of the type of the Korteweg–de Vries–Burgers (KdV–B) [37], Boussinesq [32] and Womersley equations [64]. In neuronal dynamics, electric signals in nerves and cardiac myocytes can be mathematically modeled by the Burgers–Huxley (BH) PDE [93].

Exact and approximate results are exhibited, utilizing traveling wave, periodic wave and similarity transforms, as well as by implementing the hyperbolic tangent and factorization methods [2, 27, 65, 99]. Semi-exact solutions are derived, using a homotopy analysis approach [57, 58]. A computational spectral Fourier approach [2, 6, 87] is discussed and tested, emphasizing to applications to fluid mechanics. Solitary wave interactions are examined for the BBM, CH

and DP PDEs. Multi-shock fusion is presented for the viscous Burgers PDE. Line solitons are obtained for the KP PDE. The Davey–Stewartson (DS) equation is also studied, emphasizing to fluid dynamics applications [50, 68].

Phase plane analysis is performed for the CH, DP and KdV–B equations. Weak solution formulation is presented for the CH, DP and inviscid Burgers equations and the qualitative behavior of scalar hyperbolic conservative forms is examined. The Rankine–Hugoniot and entropy conditions are discussed in implementating the method of characteristics. Lax pairs, along with the IST and UTM, are briefly discussed. The Cole–Hopf Transform is described, converting the viscous Burgers PDE to the linear Heat transport PDE, solving its most general Cauchy problem.

CHAPTER 2

Pulsatile Arterial Flow - The Womersley and KdV–B Equations

2.1 The Womersley equation

In fluid dynamics, the pulsatile, or as more commonly known, the Womersley flow, is a flow governed by periodic variations. Womersley was the first to derive such flow profiles in his study of arterial blood flow [98]. Pulsatile flow can efficiently mathematically model the cardiovascular system of chordate animals, yet it's also observed in engines and hydraulic systems, as a result of rotating and pumping mechanisms. Pulsatile flow profiles are governed by the Womersley equation, describing an unsteady flow velocity profile in a straight circular tube of length l and radius R, filled with a fluid of density ρ and viscosity μ.

In steady flow, if ρ_1 and ρ_2 are the pressures at the ends of the tube, the pressure gradient is $\dfrac{\rho_1 - \rho_2}{l}$. Let $w = w(r,t)$ denote the longitudinal flow at axial distance r and time t. In this case, w follows the Hagen–Poiseuille flow [83],

$$w(r,t) = \frac{\rho_1 - \rho_2}{4\mu l}\left(R^2 - r^2\right). \tag{2.1}$$

Setting,

$$y := \frac{r}{R}, \tag{2.2}$$

transforms (2.1) into,

$$w(y,t) = \frac{\rho_1 - \rho_2}{4\mu l} R^2\left(1 - y^2\right), \tag{2.3}$$

with y denoting the dimensionless scaled distance.

Derivation of the exact solution of the unsteady flow velocity profile, demands taking the following assumptions [71].

1. The fluid is homogeneous, incompressible and Newtonian.
2. The tube wall is rigid and circular.
3. The motion is laminar, axisymmetric and parallel to the tube's axis.
4. Axisymmetry and no-slip condition hold at the tube's centre and on the its wall, respectively.
5. The pressure gradient is periodic in time.
6. Gravitation has no effect on the fluid.

Under the above considerations, the Navier–Stokes equations simplify to,

$$\rho\frac{\partial w}{\partial t} = \frac{\partial p}{\partial x} + \mu\left(\frac{\partial^2 w}{\partial r^2} + \frac{1}{r}\frac{\partial w}{\partial r}\right) \tag{2.4}$$

and

$$\frac{\partial w}{\partial x} = 0. \tag{2.5}$$

Consider a varying pressure gradient,

$$\frac{\partial p}{\partial x}(t) = \frac{\rho_1 - \rho_2}{l} := A\mathrm{e}^{int} \tag{2.6}$$

with frequency,

$$\omega = \frac{n}{2\pi}. \tag{2.7}$$

The latter is justified by the cardiac pulse being time-periodic, and thus expressable as a series of terms of the above form. The equation of motion, (2.4), becomes,

$$\frac{\partial^2 w}{\partial r^2} + \frac{1}{r}\frac{\partial w}{\partial r} - \frac{1}{\nu}\frac{\partial w}{\partial t} = -\frac{A}{\mu}\mathrm{e}^{int} \tag{2.8}$$

with $\nu = \frac{\mu}{\rho}$ being the kinematic viscosity of the fluid. Incompressibility of the fluid allows considering the separation of variables,

$$w(r,t) = u(r)\mathrm{e}^{int}, \tag{2.9}$$

transforming (2.8) into,

$$r^2\frac{d^2u}{dr^2}+r\frac{du}{dr}+\frac{i^3n}{\nu}r^2u=-\frac{A}{\mu}r^2. \tag{2.10}$$

Setting,

$$\begin{cases} u:=\dfrac{\nu}{n}v, \\ r:=x\sqrt{\dfrac{\nu}{n}} \end{cases} \tag{2.11}$$

transforms (2.10) into,

$$x^2\frac{d^2v}{dx^2}+x\frac{dv}{dx}+\left(i^{3/2}x\right)^2v=-\frac{A}{\mu}x^2. \tag{2.12}$$

The homogeneous equation of (2.12), being a Bessel equation [8], is solvable by the Frobenius method [84]. Notice that,

$$v_p=\frac{A}{\mu i} \tag{2.13}$$

is particular solution of (2.12). The boundary conditions are axisymmetry at the centre and no-slip condition on the wall, translating for v to,

$$\begin{cases} v\left(R\sqrt{\dfrac{n}{\nu}}\right)=0, \\ \\ \dfrac{dv}{dx}(0)=0 \end{cases} \tag{2.14}$$

In that case, the solution may be written as,

$$u(r,t)=\frac{A}{\rho ni}\left\{1-\frac{J_0\left(r\sqrt{\dfrac{n}{\nu}}i^{3/2}\right)}{J_0\left(R\sqrt{\dfrac{n}{\nu}}i^{3/2}\right)}\right\} \tag{2.15}$$

where $J_0(\cdot)$ is the Bessel function of first kind and order zero [8].

Remark 1. *Since* (2.12) *is linear, the velocity profile itself is obtained by taking the real part of the complex function resulted from the summation of all harmonics of the pulse.*

Definition 1. *[98] The non-dimensional quantity,*

$$R\sqrt{\frac{n}{\nu}}, \tag{2.16}$$

expressing the pulsatile flow frequency in relation to viscous effects, is defined as the Womersley number and is denoted with α or Wo. Additionally, it maintains dynamic similarity when scaling up the cardiovascular system for experimental study.

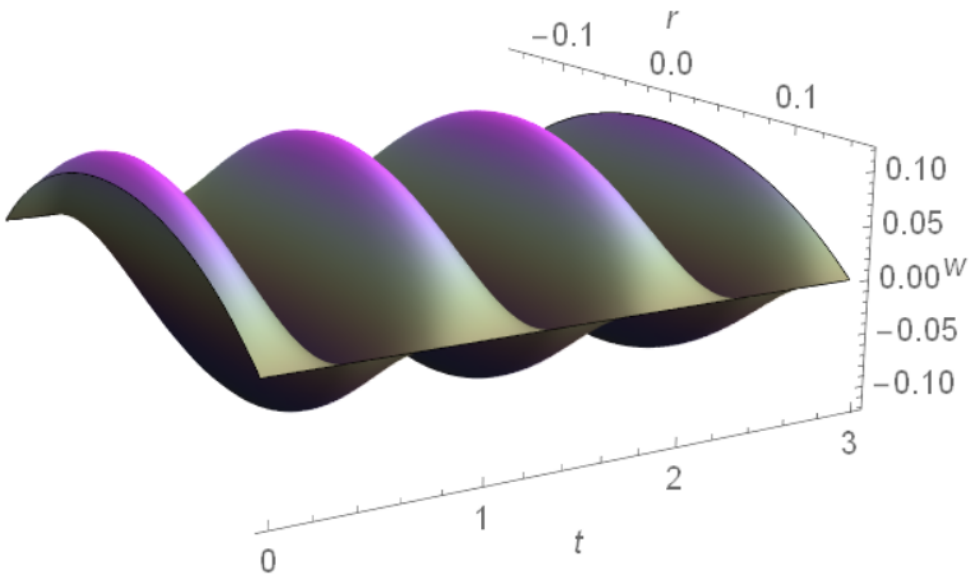

Figure 2.1: A pulsatile velocity profile of the Womersley equation, for the values of $A = 1$, $R = 0.15$, $\rho = 1.05$, $\mu = 0.04$ and $n = 2\pi$, indicating a Womersley number of $Wo = 1.926$ and a pulse frequency of $\omega = 1$ [98].

Remark 2. *The specified values of the flow for Figure 2.1, may mathematically model blow flow in the human cardiovascular system, where a pulse is generated approximately once per second.*

Remark 3. *For $Wo \lesssim 2$, viscous forces the flow is dominated by viscous forces and the flow profile is parabolic. However, in case $Wo \gtrsim 2$, the central core is dominated by inertial forces and the boundary layer by viscous forces [71, 98].*

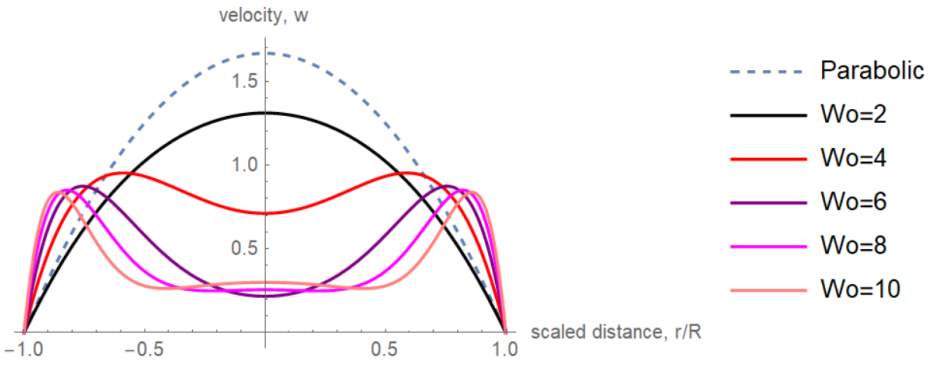

Figure 2.2: Velocity profiles for distinct Womersley values. The parabolic profile originates from the Hagen–Poiseuille flow.

2.1.1 Flow rate

The rate of flow, or equivalently, the quantity of liquid passing through any cross section per unit time, is,

$$\begin{aligned} Q &= 2\pi \int_0^R wr \; dr \\ &\overset{(2.2)}{=} 2\pi R^2 \int_0^1 wy \; dy \\ &\overset{(2.15)}{=} \frac{2\pi A}{\rho n i} \left\{ \frac{R^2}{2} - \frac{R^2}{J_0\left(\alpha i^{3/2}\right)} \int_0^1 J_0\left(\alpha y i^{3/2}\right) y \; dy \right\} \mathrm{e}^{int}. \end{aligned} \tag{2.17}$$

Since,

$$\frac{d}{dx}\left[x \, J_1(x)\right] = x \, J_0(x), \tag{2.18}$$

is a known property of Bessel functions [8], one finally obtains,

$$Q = \frac{\pi R^2 A}{\rho n i} \left\{ 1 - \frac{2\alpha i^{3/2} J_1\left(\alpha i^{3/2}\right)}{i^3 \alpha^2 J_0\left(\alpha i^{3/2}\right)} \right\} \mathrm{e}^{int}. \tag{2.19}$$

2.1.2 The transition to the KdV–B equation

Solitons are mathematical entities appearing as solutions of nonlinear wave equations [20]. They are waves of stable and steady form, although internal

oscillations may occur, exhibiting unique characteristics when colliding with other solitary waves as described by Ablowitz and Segur [7].

An increasing number of studies focuses on describing the cardiac pulse as a soliton, due to the features those two seem to share. In the arterial tree, pulse velocity is proportional to arterial width. Additionally, the arterial pressure waveform widens when propagating from wider to narrower arteries, maintaining its form as the mean arterial pressure drops [64].

The controllable synchronization effect, in the pulsatility of the smooth arterial muscle, has allowed discussing on solitary waveforms modeling cardiac dynamics [76, 64]. The stages of maximum flow and dicrotic notch, in the formation of the cardiac pulse, reveal a combination of solitary and shock wave characteristics [11, 35, 64, 99].

Blood is studied as an incompressible fluid, a characterization justified by its compressibility being rather insignificant, compared to the dilation of the blood vessels. Lambert based on the Euler equations of fluid motion, proposed the Method of Characteristics for the calculations concerning the nonlinear blood flow. By then, all related models had been one-dimensional [81].

Yomosa and collaborators proposed a theory describing solitons in long arteries, where the viscous effects, the reflective effects caused by the arterial branch as well as the effects of the peripheral resistance are neglectible. For the above reasons, the latter modulation is unable to describe the pressure drop caused when moving away from the heart. Nevertheless, it points out that it does make some sense to attribute the special features of the pulsatile wave, including the "sudden steepening" and the change in the phase velocity, to the solitary profile [64].

Gradually, a plethora of researchers examined propagating waves in a thin elastic tube, under an initial stress distribution [11]. Most of these studies, considered dispersive waves of small width [30]. Demiray and Erbay, analyzing propagating waves in a thin viscoelastic tube, were lead to the KdV–B equation [30, 35].

All of these studies, assumed both an inviscid fluid and a neglectable axial movement of the tube's wall. However, regarding biological applications, blood is both incompressible and viscous, so Antar and Demiray formulated their mathematical model toward this direction [11]. Blood flow dynamics, modeled by KdV–B- and Boussinesq-type equations, remains an active research field [16, 51, 64].

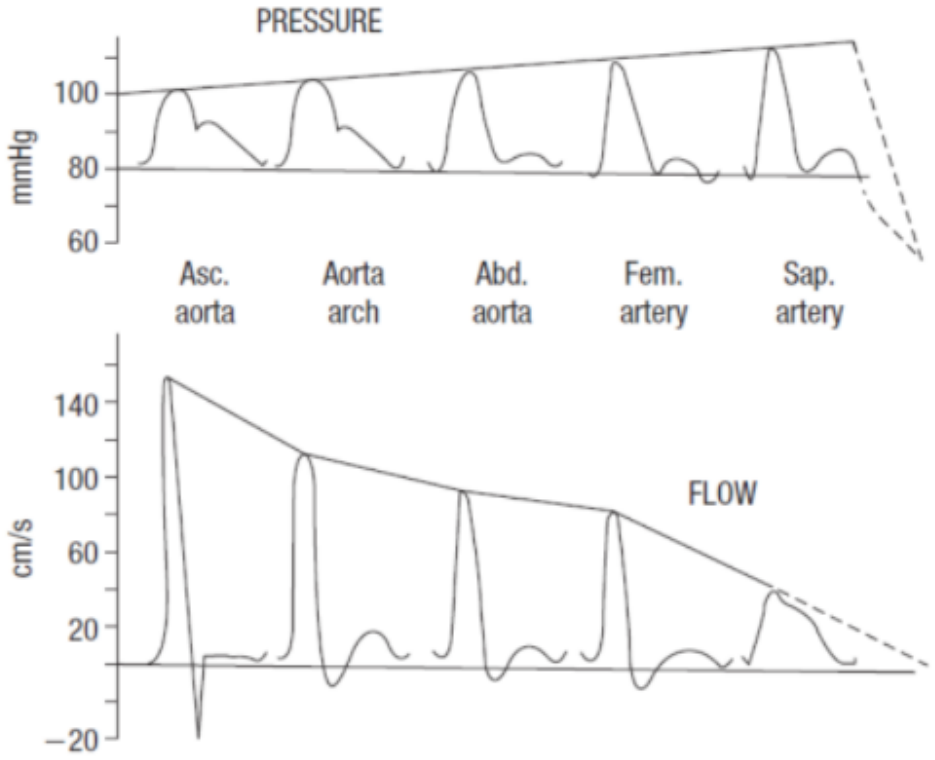

Figure 2.3: Arterial pressure and flow waveforms [64].

2.2 The Korteweg–de Vries–Burgers equation

In this section, an emphasis is given to the theoretical and qualitative analysis of the Korteweg–de Vries–Burgers (KdV–B) equation [99],

$$u_t + \gamma u u_x - \alpha u_{xx} + \beta u_{xxx} = 0, \quad u = u(x,t), \quad (x,t) \in \mathbb{R} \times (0,\infty). \quad (2.20)$$

The equation serves as the simplest nonlinear and nonintegrable wave model balancing nonlinearity, dissipation and dispersion. A derivation of the model, comes through considering the Womersley flow assumptions, along with a thin and viscoelastic tube [30, 35]. Focus shall be set on its applications to cardiac hemodynamics [11, 35, 99], where the dicrotic notch stage is observed. The corresponding analytical solutions, about to be found, are in qualitative agreement with the dicrotic notch stage.

2.2.1 Phase plane analysis

The traveling wave transform, (3.8), reduces the KdV–B equation to,

$$\begin{cases} \dfrac{du}{d\zeta} = v, \\ \\ \dfrac{dv}{d\zeta} = -\dfrac{u}{\beta}\left(\dfrac{\gamma}{2}u - \lambda\right) + \dfrac{\alpha}{\beta}v. \end{cases} \tag{2.21}$$

Regarding the system's stability points, the following hold [99].

1. $(0,0)$ is invariably a saddle point.
2. For $\alpha \geq 2\sqrt{\lambda\beta}$ the point $\left(\dfrac{2\lambda}{\gamma}, 0\right)$ is a source (unstable node).
3. For $0 < \alpha < 2\sqrt{\lambda\beta}$ the point $\left(\dfrac{2\lambda}{\gamma}, 0\right)$ is a foci (unstable node).
4. For $\alpha = 0$ the point $\left(\dfrac{2\lambda}{\gamma}, 0\right)$ is a center (stable node).

The geometric nature of these points is summarized in the following [99].

1. $(0,0)$ being a saddle point, means that it's an unstable node and phase trajectories tend to move around it in hyperbolas, defined by the separatrices (i.e. straight lines directed along the two eigenvectors of the linearization matrix).
2. $((\frac{2\lambda}{\gamma}, 0) : \alpha \geq 2\sqrt{\lambda\beta})$ being a source, means that it's an unstable node from where phase trajectories diverge away without any (or relatively little) rotation.
3. $((\frac{2\lambda}{\gamma}, 0) : \alpha \in (0, 2\sqrt{\lambda\beta}))$ being a spiral source, means that it's an unstable focus where phase trajectories tend to spiral around before eventually diverge away from it.
4. $((\frac{2\lambda}{\gamma}, 0) : \alpha = 0)$ being a central point, means that the phase trajectories tend to move in ellipses around the point, describing periodic motion of a point in the phase space.

2.3 The hyperbolic tangent method

Since the late 1980s, notable research has been done on analytical solutions of the KdV–B equation [31, 91]. Results on the respected Cauchy problem, addressing existence and uniqueness, can be found on [18]. Notable results regarding the 2-dimensional KdV–B equation can be found on [37].

Traveling wave solutions of the n-dimensional KdV–B and compound KdV–B equations ($n \in \mathbb{N}$) will be derived through the hyperbolic tangent, or Tanh, method [40, 45, 65, 95, 99]. Conclusions will be drawn on the method's applicability to nonlinear evolution PDEs.

2.3.1 The KdV–B equation

Consider the traveling wave transform of u,

$$\begin{cases} u(x,t) = u(\zeta), \\ \zeta = \mu(x - \lambda t), \quad \mu > 0, \quad \lambda \neq 0 \end{cases} \tag{2.22}$$

Here, μ represents the wave number and λ the, perhaps unknown, velocity. Recall that μ is inversely proportional to the wave's width [4, 5].

Now, (2.22) transforms the KdV–B equation, (2.20), into the ODE for $u(\zeta)$,

$$-\lambda u'(\zeta) + \gamma u(\zeta) u'(\zeta) - \alpha\mu u''(\zeta) + \beta\mu^2 u'''(\zeta) = 0. \tag{2.23}$$

Integrating (2.23), yields,

$$-\lambda u(\zeta) + \frac{\gamma}{2} u^2(\zeta) - \alpha\mu u'(\zeta) + \beta\mu^2 u''(\zeta) = C. \tag{2.24}$$

The concept behind the Tanh method lies on the key-property of the tanh function's derivatives all being written in terms of the tanh function itself. The rather useful identity is used,

$$\operatorname{sech}^2\zeta = 1 - \tanh^2\zeta, \quad \zeta \in \mathbb{R}. \tag{2.25}$$

The above transform the studied differential equation to a polynomial equation for successive powers of the tanh function.

Introducing the new variable,

$$y = \tanh\zeta, \tag{2.26}$$

the solution(s) seeked shall take the form,

$$u(y) = \sum_{n=0}^{N} a_n y^n, \tag{2.27}$$

limiting them to solitary and shock wave profiles. Chain differentiation provides with,

$$\begin{cases} \dfrac{d}{d\zeta} = \dfrac{d}{dy}\dfrac{dy}{dz} = \mu(1-y^2)\dfrac{d}{dy}, \\ \dfrac{d^2}{d\zeta^2} = \dfrac{d}{d\zeta}\dfrac{d}{d\zeta} = \mu^2(1-y^2)\left(-2y\dfrac{d}{dy} + (1-y^2)\dfrac{d^2}{dy^2}\right) \end{cases} \tag{2.28}$$

The positive integer value of N is determined after substituting (2.27), along with (2.28), into (2.24) and balancing the resulting highest order nonlinear terms with the highest order linear terms. As a result, it's definitely required that $a_{N+1} = 0$ and $a_N \neq 0$ for a particular N. It turns out that N equals 1 or 2 in most cases.

As soon as N is determined in this way, substitution of (2.27) into (2.24) produces an algebraic system for a_n, $n = 0, 1, \ldots, N$. Based on the problem under study, the μ either remains fixed or undetermined, whereas the velocity λ is always a function of μ.

In the present study, $N = 2$, hence substituting (2.27) into (2.24) and setting the like powers of equal to zero, one obtains the following solutions,

$$\begin{cases} \lambda = \pm\dfrac{\sqrt{2}\sqrt{18\alpha^4 - 625C\beta^2\gamma}}{25\beta}, \\ \mu = \dfrac{\alpha}{10\beta}, \\ a_0 = \dfrac{3\alpha^2 + 25\beta\lambda}{25\beta\gamma}, \\ a_1 = -\dfrac{6\alpha^2}{25\beta\gamma}, \\ a_2 = -\dfrac{3\alpha^2}{25\beta\gamma}. \end{cases} \tag{2.29}$$

Combining (2.29) with (2.27), while using (2.26), provides with,

$$u(\zeta) = \frac{\lambda}{\gamma} + \frac{3\alpha^2\left(\operatorname{sech}^2\zeta - 2\tanh\zeta\right)}{25\beta\gamma}. \tag{2.30}$$

Remark 4. *The solution consists of both solitary and shock parts, a behavior also highlighted in the formational stages of the cardiac pulse [99].*

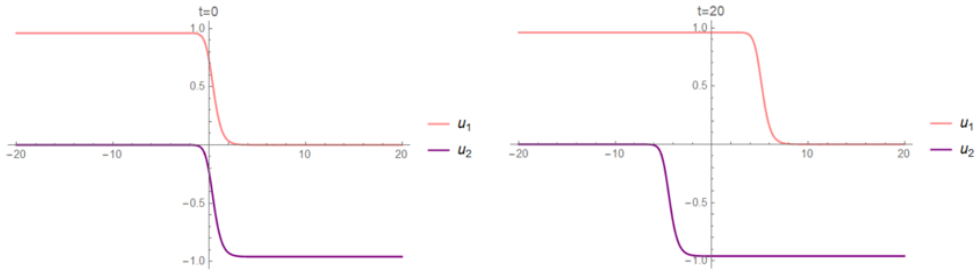

Figure 2.4: A right- (u_1) and left-moving (u_2) wavefront solutions of KdV–B, for the values of $\alpha = 0.1$, $\beta = 0.01$ and $\gamma = 0.5$, with $x \in [-20, 20]$ and $t \in \{0, 20\}$.

2.3.2 The 2-dimensional KdV–B equation

Consider the 2-dimensional KdV–B equation [37],

$$\left(u_t + \gamma u u_x - \alpha u_{xx} + \beta u_{xxx}\right)_x + u_{yy} = 0, \quad u = u(x, y, t). \tag{2.31}$$

Application of the traveling wave transform,

$$\begin{cases} u = u(\zeta), \\ \zeta = \mu(x + y - \lambda t), \quad \mu > 0, \quad \lambda \neq 0 \end{cases} \tag{2.32}$$

transforms, through chain differentiation, the 2-dimensional KdV–B equation into,

$$\left(-\lambda u' + \gamma u u' - \alpha\mu u'' + \beta\mu^2 u'''\right)' + u'' = 0, \quad u = u(\zeta). \tag{2.33}$$

Double integration with respect to ζ, taking integration constants to equal zero, provides with,

$$\beta\mu^2 u'' - \alpha\mu u' + \frac{\gamma}{2}u^2 + (1 - \lambda)u = 0. \tag{2.34}$$

Under similar manipulations to those on the KdV–B case, one is led to the kink-form traveling wave solutions,

$$u(\zeta) = \frac{\lambda - 1}{\gamma} + \frac{3\alpha^2 \left(\operatorname{sech}^2\zeta - 2\tanh\zeta\right)}{25\beta\gamma} \tag{2.35}$$

with,

$$\begin{cases} \lambda = 1 \pm \dfrac{6\alpha^2}{25\beta}, \\ \\ \mu = \dfrac{\alpha}{10\beta} \end{cases} \tag{2.36}$$

2.3.3 A generalization to the n-dimensional KdV–B equation

Generalizing both (2.31) and the ideas followed in [37], one obtains the n-dimensional KdV–B equation,

$$\left(u_t + \gamma u u_{x_1} - \alpha u_{x_1x_1} + \beta u_{x_1x_1x_1}\right)_{x_1} + \sum_{i=2}^{n} u_{x_ix_i} = 0, \quad u = u(x_1, x_2, \ldots, x_n, t). \tag{2.37}$$

Consider a generalization of (2.32), of,

$$\begin{cases} u = u(\zeta), \\ \\ \zeta = \mu\left(\displaystyle\sum_{i=1}^{n} x_i - \lambda t\right), \quad \mu > 0, \quad \lambda \neq 0 \end{cases} \tag{2.38}$$

The Tanh method, applied to (2.41), provides with the traveling wave solutions,

$$u(\zeta) = \frac{\lambda - n + 1}{\gamma} + \frac{3\alpha^2 \left(\operatorname{sech}^2\zeta - 2\tanh\zeta\right)}{25\beta\gamma} \tag{2.39}$$

with,

$$\begin{cases} \lambda = n - 1 \pm \dfrac{6\alpha^2}{25\beta}, \\ \\ \mu = \dfrac{\alpha}{10\beta} \end{cases} \quad , \quad n \in \{2, \ldots\} \tag{2.40}$$

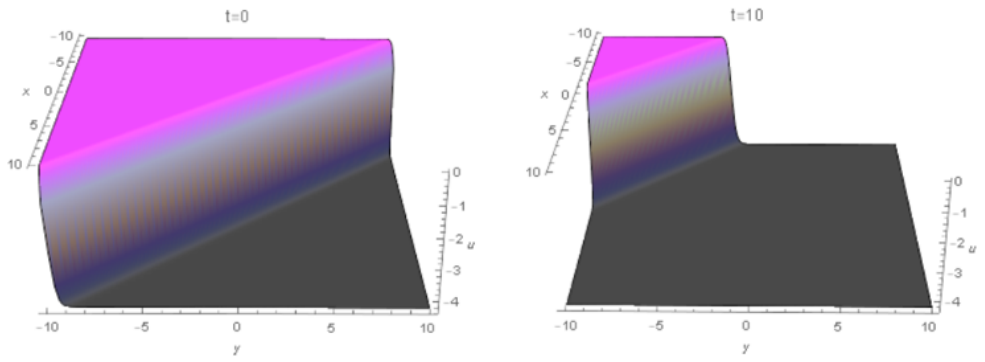

Figure 2.5: A left-moving, kink-shaped, traveling wave of 2-dimensional KdV–B, for the values of $\alpha = 0.3$, $\beta = 0.01$ and $\gamma = 1$, with $(x, y) \in [-10, 10] \times [-10, 10]$ and $t \in \{0, 10\}$.

2.3.4 The n-dimensional compound KdV–B equation

Consider the n-dimensional compound KdV–B (cKdV–B) PDE,

$$\left(u_t + \gamma u u_{x_1} - \delta u^2 u_{x_1} - \alpha u_{x_1 x_1} + \beta u_{x_1 x_1 x_1}\right)_{x_1} + \sum_{i=2}^{n} u_{x_i x_i} = 0, \quad \delta > 0 \tag{2.41}$$

along with (2.38). The equation generalizes the one presented in [37], connecting the modified KdV and Burgers PDEs. More on these two will discussed in the process. Regarding cKdV–B, one obtains $N = 1$ and the Tanh method provides with the traveling wave solution,

$$u(\zeta) = \frac{3\sqrt{\beta}\gamma + \sqrt{6}\alpha\sqrt{\delta}}{6\sqrt{\beta}\delta} + \frac{\sqrt{6}\sqrt{\beta}\mu \tanh\zeta}{\sqrt{\delta}} \tag{2.42}$$

with,

$$\begin{cases} \lambda = n - 1 + \dfrac{\gamma^2}{6\delta} - \dfrac{\alpha\left(4\alpha + \dfrac{\sqrt{6}\sqrt{\beta}\gamma}{\sqrt{\delta}}\right)}{18\beta}, \\ \mu = \dfrac{\sqrt{\dfrac{-2\alpha^2\delta + 3\beta\left(\gamma^2 + 4\delta(n - 1 - \lambda)\right)}{\beta^2\delta}}}{2\sqrt{6}} \end{cases}, \quad n \in \mathbb{N} \tag{2.43}$$

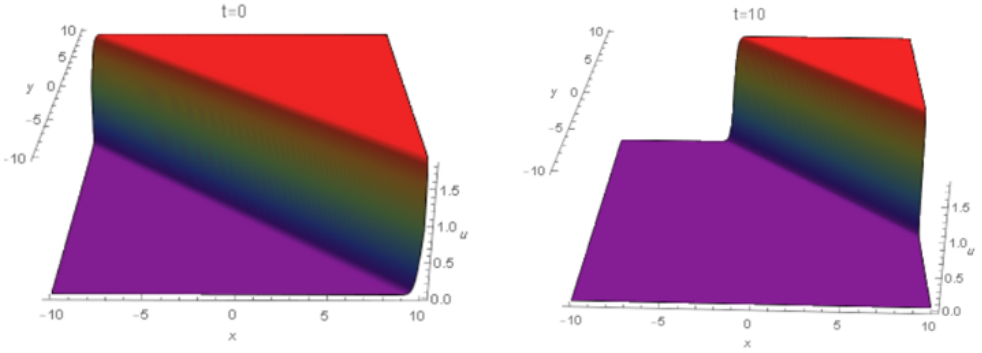

Figure 2.6: A right-moving, kink-shaped, traveling wave of the 2-dimensional compound KdV–B, for the values of $\alpha = 0.1$, $\beta = 0.01$, $\gamma = \delta = 1$, with $(x, y) \in [-10, 10] \times [-10, 10]$ and $t \in \{0, 10\}$.

Remark 5. *The Tanh method allows for a straightforward algorithmic process to derive physically relevant kink and pulse form solutions for a wide variety of PDEs. Its novelty lies in circumventing integration and obtaining closed-form solutions at the cost of some algebraic manipulations. The method led to the development of notable symbolic software packages, e.g.* ***PDESpecialSolutions.m*** *and* ***DDESpecialSolutions.m****, applying to PDEs and DDEs (Difference-Delay Equations), respectively [13].*

Remark 6. *The Tanh method, along with its improvements [41, 94] can be successfully applied to the vast majority of equations studied throughout the thesis. More on these solutions will be discussed in the process.*

CHAPTER 3

The Burgers and Kadomtsev–Petviashvili (KP) Equations

3.1 The viscous Burgers equation

The effects of diffusion and nonlinear advection are combined in the viscous Burgers PDE, most commonly written as [3, 97],

$$u_t + uu_x - \alpha u_{xx} = 0, \quad u = u(x,t), \quad (x,t) \in \mathbb{R} \times (0,\infty), \quad \alpha > 0. \tag{3.1}$$

Initially introduced by Bateman in 1915 and later studied by Burgers in 1948 [97], it mathematically models phenomena in fluid mechanics [14, 89].

More specifically, the equation mathematically models 1-dimensional viscous fluid motion, providing with the fluid velocity, u, along a thin ideal pipe as time passes. The constant α expresses the fluid's viscosity.

3.1.1 Derivation from the Navier–Stokes equations

The Burgers equation serves as a simplified model of the Navier–Stokes equations. For a Newtonian incompressible fluid, the Navier-Stokes equations, in vector form, read [14, 80, 89]

$$\rho\left(\frac{\partial \mathbf{u}}{\partial t} + \mathbf{u}\cdot\nabla\mathbf{u}\right) = -\nabla p + \mu\nabla^2\mathbf{u} + \mathbf{F}. \tag{3.2}$$

Here, ρ is the fluid density, $\mathbf{u}$ is the velocity vector field, p is the pressure, μ is the viscosity, and $\mathbf{F}$ is an external force field. Considering that the effect of

pressure drop is negligible, $\nabla p = 0$, write,

$$\rho\left(\frac{\partial \mathbf{u}}{\partial t} + \mathbf{u}\cdot\nabla\mathbf{u}\right) = \mu\nabla^2\mathbf{u} + \mathbf{F}. \tag{3.3}$$

The latter simplifies further, assuming the external force field term being zero and taking advantage of the fact that ρ is a constant for an incompressible fluid. Define a new constant, the kinematic viscosity,

$$\nu = \frac{\mu}{\rho}. \tag{3.4}$$

Combining (3.3) with (3.4), provides with,

$$\frac{\partial \mathbf{u}}{\partial t} + \mathbf{u}\cdot\nabla\mathbf{u} = \nu\nabla^2\mathbf{u}. \tag{3.5}$$

The following sections deal with the 1-dimensional viscous Burgers equation. In that case, (3.5) becomes,

$$\frac{\partial u}{\partial t} + u\frac{\partial u}{\partial x} = \nu\frac{\partial^2 u}{\partial x^2}, \tag{3.6}$$

being exactly, the 1-dimensional viscous Burgers equation.

3.1.2 Analytic traveling wave solutions

Consider the viscous Burgers equation,

$$\begin{cases} u_t + uu_x - \alpha u_{xx} = 0, \quad u = u(x,t), \quad \alpha > 0, \\ \lim\limits_{x\to-\infty} u(x,t) = u_1, \quad \lim\limits_{x\to\infty} u(x,t) = u_2, \quad u_1 > u_2, \quad \text{being two constant values} \end{cases} \tag{3.7}$$

and apply the traveling wave transform,

$$\begin{cases} u(x,t) = u(\zeta), \\ \zeta = x - \lambda t, \quad \lambda \neq 0 \end{cases} \tag{3.8}$$

Application of the chain rule, leads to,

$$-\lambda u'(\zeta) + u(\zeta)u'(\zeta) - \alpha u''(\zeta) = 0, \quad u = u(\zeta). \tag{3.9}$$

Integrating gives,

$$\begin{aligned} &-\lambda u + \frac{1}{2}u^2 - \alpha u' = C \\ &\Leftrightarrow u' = \frac{1}{2\alpha}\left(u^2 - 2\lambda u - 2C\right), \end{aligned} \tag{3.10}$$

where C is a constant of integration. Clearly, (3.10) suggests that u_1 and u_2 solve the aove quadratic. Thus, using Vieta's formulas,

$$\begin{cases} \lambda = \dfrac{u_1 + u_2}{2}, \\ \\ C = -\dfrac{u_1 u_2}{2} \end{cases} \tag{3.11}$$

At this stage, (3.10) can be rewritten as,

$$u' = \frac{1}{2\alpha}(u - u_1)(u - u_2), \tag{3.12}$$

being a first order separable equation for u. Now, integration of (3.12), taking the integration constant to equal 0, leads to,

$$u(\zeta) = \frac{u_1 + u_2 \mathrm{e}^{\frac{u_1 - u_2}{2\alpha}\zeta}}{1 + \mathrm{e}^{\frac{u_1 - u_2}{2\alpha}\zeta}}. \tag{3.13}$$

An equivalent form for u, using trigonometric arguments, is,

$$\frac{(u_1 + u_2)}{2} - \frac{(u_1 - u_2)}{2} \tanh\left(\frac{(u_1 - u_2)}{4\alpha}\zeta\right). \tag{3.14}$$

At $\zeta = 0$, notice that,

$$u = \frac{u_1 + u_2}{2}. \tag{3.15}$$

The presence of diffusion, α, is of great importance, since it prevents any wave distortion. On the other hand, if the diffusion term is absent ($\alpha \to 0^+$), the solution becomes discontinuous, with,

$$\lim_{\alpha \to 0^+} u(x,t) = \begin{cases} u_1, & x < \dfrac{(u_1 + u_2)}{2} t, \\ \\ u_2, & x > \dfrac{(u_1 + u_2)}{2} t \end{cases} \tag{3.16}$$

Remark 7. *The advantage of the above analysis is that the convection and diffusion terms in the Burgers equation exhibit opposite effects.*

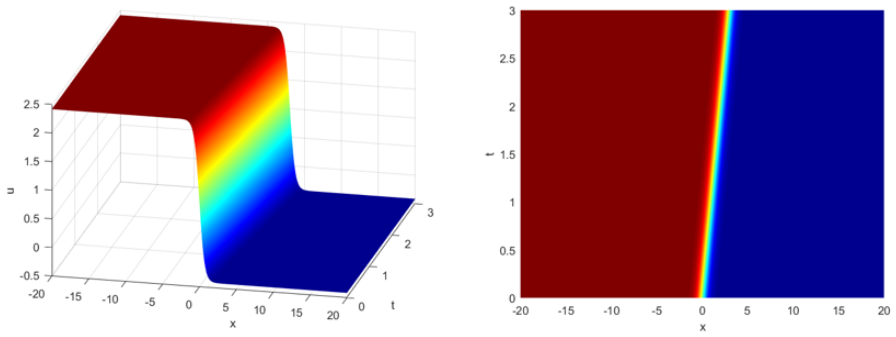

Figure 3.1: A traveling wave solution of the viscous Burgers equation, for the values of $\alpha = 0.5$, $u_1 = 1+\sqrt{2}$ and $u_2 = 1-\sqrt{2}$, with $(x,t) \in [-20,20] \times [0,3]$.

3.1.3 Multi-shock fusion

Consider the N-shock solution of the viscous Burgers equation,

$$u_N(x,t) = -2\frac{\sum_{i=1}^{N} \kappa_i \mathrm{e}^{\frac{\kappa_i}{\alpha}(x+\kappa_i(t-t_0))}}{1+\sum_{i=1}^{N} \mathrm{e}^{\frac{\kappa_i}{\alpha}(x+\kappa_i(t-t_0))}}. \tag{3.17}$$

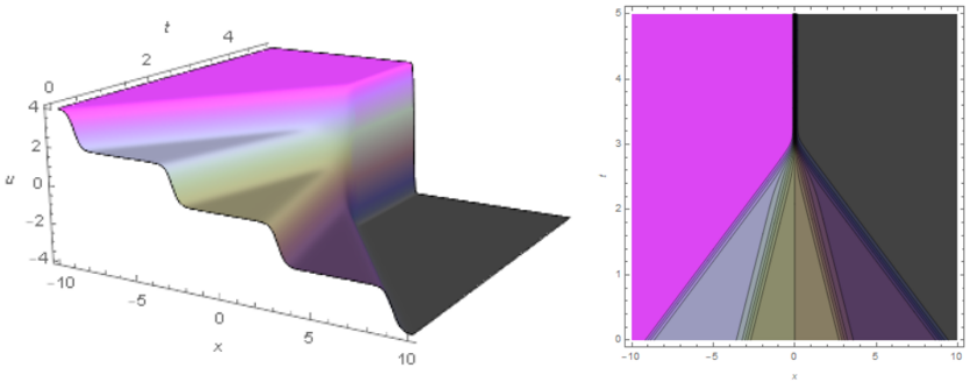

Figure 3.2: A multi-shock solution, for the values of $N = 4$, $\alpha = 0.2$, $\kappa_1 = 2$, $\kappa_2 = -1$, $\kappa_3 = 1$, $\kappa_4 = -2$ and $t_0 = 3$, with $(x,t) \in [-10,10] \times [0,5]$.

The above demonstrates different shock traveling waves, propagating at opposite directions, colliding at time t_0 forming a sole shock wave. A specific case, for $N = 2$, is discussed in detail in [79, 92].

Remark 8. *Multi-shock interactions, are of great importance in aerospace engineering. They are mainly applied to re-entry vehicles, launcher-booster interaction and engine inlets [72].*

3.1.4 Self-similar solutions

The nontrivial self-similar solutions shall be given by,

$$\begin{cases} u(x,t) = t^m f(h), \\ mf(h) + nhf'(h) + t^{m+n+1} f(h)f'(h) - \alpha t^{2n+1} f''(h) = 0, \quad h = xt^n \end{cases} \tag{3.18}$$

reducing to an ODE, for $f(h)$, provided,

$$m = n = -\frac{1}{2}. \tag{3.19}$$

Thus, the equation under study shall be,

$$\alpha f''(h) + \frac{1}{2}\left(f(h) + hf'(h)\right) - f(h)f'(h) = 0. \tag{3.20}$$

Integration, respecting vanishing infinity conditions, yields,

$$\begin{aligned} \alpha f'(h) + \frac{1}{2}\left(hf(h) - f^2(h)\right) &= 0 \\ \overset{\alpha \gtrless 0}{\Leftrightarrow} f'(h) = -\frac{h}{2\alpha} f(h) + \frac{1}{2\alpha} f^2(h). \end{aligned} \tag{3.21}$$

Now, (3.21) is a first order Bernoulli equation. Seeking for nontrivial solutions, start by dividing both sides of (3.21) by $f^2(h)$, obtaining,

$$f^{-2}(h)f'(h) = -\frac{h}{2\alpha} f^{-1}(h) + \frac{1}{2\alpha}. \tag{3.22}$$

Finally, setting,

$$v(h) = f^{-1}(h), \tag{3.23}$$

(3.22) reads,

$$v'(h) = \frac{h}{2\alpha} v(h) - \frac{1}{2\alpha}, \tag{3.24}$$

with its general solution being,

$$v(h) = \mathrm{e}^{\frac{h^2}{4\alpha}} \left(C - \frac{\sqrt{\pi}}{2\sqrt{\alpha}} erf\left(\frac{h}{2\sqrt{\alpha}}\right)\right). \tag{3.25}$$

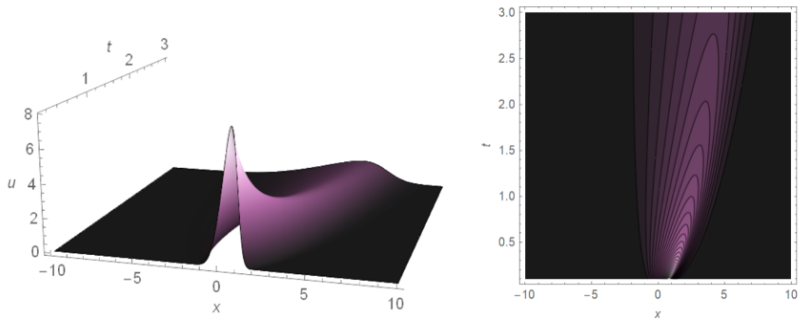

Figure 3.3: A self-similar solution of the viscous Burgers equation, for the values of $\alpha = 0.8$ and $C = 1$, with $(x,t) \in [-10,10] \times [0.1,3]$.

3.1.5 The Cole–Hopf Transform

The focus is now turned on the general Cauchy problem,

$$\begin{cases} u_t + uu_x - \alpha u_{xx} = 0, \quad u = u(x,t), \quad (x,t) \in \mathbb{R} \times (0,\infty), \quad \alpha > 0, \\ \\ u(x,0) = f(x) \to 0, \quad \text{as} \quad |x| \to \infty \end{cases} \tag{3.26}$$

Setting, Setting,

$$\begin{cases} w := \displaystyle\int_0^x u(y,t)\ dy, \\ h(x) := \displaystyle\int_0^x f(y)\ dy, \end{cases} \tag{3.27}$$

with $w \to$ constant as $|x| \to \infty$, leads to the Cauchy problem,

$$\begin{cases} w_t + \dfrac{1}{2} w_x^2 - \alpha w_{xx} = 0, \quad (x,t) \in \mathbb{R} \times (0,\infty), \\ \\ w(x,0) = h(x), \quad x \in \mathbb{R} \end{cases} \tag{3.28}$$

Assume, momentarily, that w is a smooth solution of (3.28), and set,

$$v = \phi(w), \tag{3.29}$$

where ϕ shall be determined in a way that v solves a linear equation.

Chain differentiation of (3.29) provides with,

$$\begin{cases} v_t = \phi'(w) w_t, \\ \\ v_{xx} = \phi''(w) w_x^2 + \phi'(w) w_{xx} \end{cases} \tag{3.30}$$

Now, as a consequence, (3.28) implies,

$$\begin{aligned} v_t &= \phi'(w) \left(\alpha w_{xx} - \frac{w_x^2}{2} \right) \\ &= \alpha v_{xx} - \left(\alpha \phi''(w) + \frac{\phi'(w)}{2} \right) w_x^2 \\ &= \alpha v_{xx}, \end{aligned}$$

provided choosing ϕ such that,

$$\alpha \phi'' + \frac{\phi'}{2} = 0. \tag{3.31}$$

The latter is solved if setting,

$$\phi = \mathrm{e}^{-\frac{z}{2\alpha}}. \tag{3.32}$$

Therefore, in case w solves (3.28), then,

$$v = \mathrm{e}^{-\frac{w}{2\alpha}}, \tag{3.33}$$

solves the Cauchy problem for the Heat transfer equation, with conductivity α,

$$\begin{cases} v_t - \alpha v_{xx} = 0, \quad (x,t) \in \mathbb{R} \times (0, \infty), \\ \\ v(x,0) = \mathrm{e}^{-\frac{h(x)}{2\alpha}} \end{cases} \tag{3.34}$$

Definition 2. *[3, 36] The formula* (3.33) *is known as the Cole–Hopf transform.*

At this point, the linear problem (3.34), admits a unique bounded solution,

$$v(x,t) = \frac{1}{\sqrt{4\pi\alpha t}} \int_{-\infty}^{\infty} \mathrm{e}^{-\frac{(x-y)^2}{4\alpha t} - \frac{h(y)}{2\alpha}} \, dy, \quad (x,t) \in \mathbb{R} \times (0, \infty). \tag{3.35}$$

Now, since (3.33) may be rewritten as,

$$w = -2\alpha \log v, \tag{3.36}$$

the explicit formula for w,

$$w(x,t) = -2\alpha \log \frac{1}{\sqrt{4\pi\alpha t}} \int_{-\infty}^{\infty} \mathrm{e}^{-\dfrac{(x-y)^2}{4\alpha t} - \dfrac{h(y)}{2\alpha}}\, dy, \quad (x,t) \in \mathbb{R} \times (0,\infty), \tag{3.37}$$

is obtained. Finally, regarding the initial unknown function, u, (3.27) along with differentiation of (3.37), gives,

$$u(x,t) = \frac{\displaystyle\int_{-\infty}^{\infty} \frac{x-y}{t} \mathrm{e}^{-\dfrac{(x-y)^2}{4\alpha t} - \dfrac{h(y)}{2\alpha}}\, dy}{\displaystyle\int_{-\infty}^{\infty} \mathrm{e}^{-\dfrac{(x-y)^2}{4\alpha t} - \dfrac{h(y)}{2\alpha}}\, dy}. \tag{3.38}$$

3.2 The Burgers–Huxley equation

Consider the Burgers–Huxley model [93],

$$u_t + u^{\kappa} u_x = u_{xx} + u^m \left(1 - u^n\right), \quad \kappa, m, n \in \mathbb{N}. \tag{3.39}$$

The model generalizes Burgers equation, in describing processes governed by reaction mechanisms. Focus is set to applications to neuronal dynamics, mainly to the description of electric pulses in neurons and cardiac myocytes.

3.2.1 The factorization method

The factorization method [27], applies to PDEs reducible to ODEs of the form,

$$u'' + f(u)u' + g(u) = 0, \quad u = u(\zeta). \tag{3.40}$$

The reduction is usually performed by a traveling wave transform, for example by (3.8). Defining two auxiliary functions, g_1 and g_2, implicitly depending on g, allows factorizing (3.40) as,

$$\left[\frac{d}{d\zeta} - g_2\right] \left[\frac{d}{d\zeta} - g_1\right] u = 0. \tag{3.41}$$

Expanding the latter, using chain differentiation, provides with,

$$u'' - g_1 u' - \frac{dg_1}{du} u' u - g_2 u' + g_1 g_2 u = 0 \tag{3.42}$$

or equivalently to [27],

$$u'' - \left(\frac{dg_1}{du} u + g_1 + g_2 \right) u' + g_1 g_2 u = 0. \tag{3.43}$$

Comparing (3.43) with (3.40), leads to,

$$\begin{cases} f(u) = -\left(\dfrac{dg_1}{du} u + g_1 + g_2 \right), \\ g(u) = g_1 g_2 u \end{cases} \tag{3.44}$$

The latter scheme provides with information on the unknown terms, whereas a compatibility between,

$$\left[\frac{d}{d\zeta} - g_1 \right] u = 0 \tag{3.45}$$

and (3.40) is established. Therefore, solving (3.45) leads to solutions of (3.40), and ultimately to solutions of the original PDE.

3.2.2 Analytic traveling wave solutions

Consider the case of $\kappa = m - 1 = n = p$. Application of (3.8), converts (3.39) into,

$$u'' + (\lambda - u^p)\, u' + u^{p+1} (1 - u^p) = 0. \tag{3.46}$$

Set,

$$\begin{cases} f(u) := \lambda - u^p, \\ g(u) := u^{p+1} (1 - u^p), \\ g_1 := q (1 - u^p), \\ g_2 := \dfrac{u^p}{q} \end{cases} \tag{3.47}$$

and apply the factorization method to obtain the right-moving traveling wave,

$$u(x,t) = \left[1 - \frac{1}{1 + \mathrm{e}^{(q(x+qt)p + Cp)}} \right]^{\frac{1}{p}} \tag{3.48}$$

with,

$$q = \frac{-1 - \sqrt{5 + 4p}}{2(p+1)}, \quad p \in \{1, 2, \ldots\}, \quad C \in \mathbb{R}. \tag{3.49}$$

A]

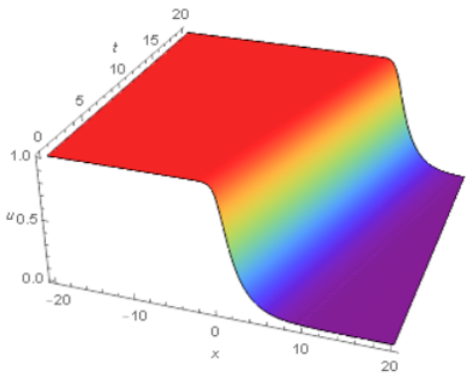

B]

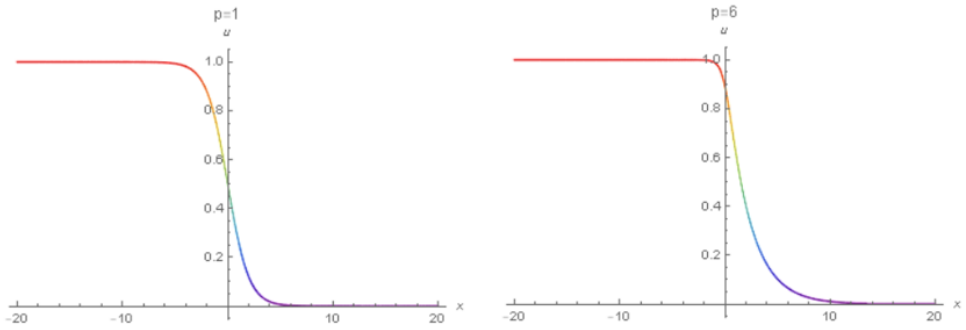

Figure 3.4: [A] A right-moving wavefront of BH, for the values of $p = 5$ and $C = 0$, with $(x, t) \in [-20, 20] \times [0, 20]$. [B] Different wavefronts of BH, for the values of $p \in \{1, 6\}$ and $C = 0$, with $(x, t) \in [-20, 20] \times \{0\}$.

3.3 The Kadomtsev–Petviashvili (KP) equation

In mathematical physics, the KP PDE [7, 47],

$$(u_t + \gamma u u_x + \beta u_{xxx})_x + 3\delta^2 u_{yy} = 0, \quad u = u(x, y, t), \quad \gamma \neq 0, \quad \beta > 0, \quad \delta^2 = \pm 1 \tag{3.50}$$

mathematically models nonlinear wave motion. Kadomtsev and Petviashvili derived it in 1970, naturally extending the pre-existing KdV [54]. Its applications range from fluid dynamics to ferromagnetism and blood flow dynamics [46, 47, 63, 64].

The case of $\delta = 1$ is known as KPII equation, whereas the $\delta = i$ case as the KPI equation. Like in the KdV case, the coefficients of KP can, under appropriate rescallings, take any arbitrary value [7].

3.3.1 Analytic line soliton solutions

Consider the traveling wave transform,

$$\begin{cases} u(x,t) = u(\zeta), \\ \zeta = x + y - \lambda t, \quad \lambda > 0 \end{cases} \tag{3.51}$$

transforming the KP into,

$$\left(-\lambda u' + \gamma u u' + \beta u'''\right)' + 3\delta^2 u'' = 0, \quad u = u(\zeta). \tag{3.52}$$

Seeking for pulse-form solutions, consider a vanishing behavior, of both u and its spatial derivatives, at both infinity. Double integration with respect to ζ, provides with,

$$u'' + \frac{(3\delta^2 - \lambda)}{\beta} u + \frac{\gamma}{2\beta} u^2 = 0, \quad u = u(\zeta). \tag{3.53}$$

Multiplication with u' and integration, leads to,

$$\frac{du}{d\zeta} = \pm\sqrt{\beta} u \sqrt{(\lambda - 3\delta^2) - \frac{\gamma}{3} u}. \tag{3.54}$$

The latter along with sech being an even function, implies that,

$$u(\zeta) = \frac{3(\lambda - 3\delta^2)}{\gamma} \operatorname{sech}^2\left(\frac{\sqrt{\lambda - 3\delta^2}}{2\sqrt{\beta}}(\zeta - c)\right), \quad c \in \mathbb{R}. \tag{3.55}$$

3.3.2 A generalization to the n-dimensional KP equation

Consider a n-dimensional KP of the form,

$$\left(u_t + \gamma u u_{x_1} + \beta u_{x_1 x_1 x_1}\right)_{x_1} + 3\delta^2 \sum_{i=2}^{n} u_{x_i x_i} = 0, \quad u = u(x_1, x_2, \ldots, x_n, t) \tag{3.56}$$

along with the traveling wave transform,

$$\begin{cases} u = u(\zeta), \\ \\ \zeta = \left(\sum_{i=1}^{n} x_i - \lambda t \right), \quad \lambda > 0 \end{cases} \tag{3.57}$$

In a similar manner with the 2-dimensional KP case, (3.56) admits a right-moving soliton of the form,

$$u(\zeta) = \frac{3(\lambda - 3(n-1)\delta^2)}{\gamma} \operatorname{sech}^2 \left(\frac{\sqrt{\lambda - 3(n-1)\delta^2}}{2\sqrt{\beta}} \zeta \right) \tag{3.58}$$

for,

$$\lambda \geq 3(n-1)\delta^2, \quad c \in \mathbb{R}, \quad n \in \{2, \ldots\}. \tag{3.59}$$

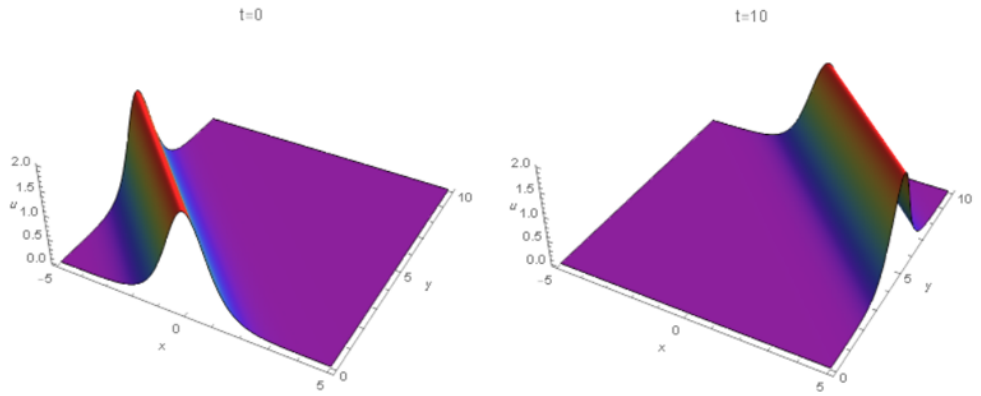

Figure 3.5: A line-soliton of the KP equation, for the values of $\lambda = \beta = 1$, $\gamma = 6$, $\delta = i$ and $c = 0$ with $(x, y) \in [-5, 5] \times [0, 10]$ and $t \in \{0, 10\}$.

CHAPTER 4

Conservative Forms - The Inviscid Burgers Equation

4.1 The inviscid Burgers equation

A phenomenon, known as "blow-up", often causes solutions of nonlinear evolution equations to exist locally, yet not globally in time. Unlike linearity, nonlinearity may cause a discontinuity to form despite a continuous initial-data, but also an initial discontinuity to be immediately resolved. Among the simplest PDEs, suffering a blow-up, is the inviscid Burgers PDE [36, 82],

$$\begin{cases} u_t + \gamma \left(\frac{u^2}{2}\right)_x = 0, \quad u = u(x,t) \in \mathbb{R}, \quad (x,t) \in \mathbb{R} \times (0,\infty), \\ u(x,0) = g(x), \quad (x,t) \in \mathbb{R} \times \{t = 0\} \end{cases} \tag{4.1}$$

Without loss of generality, assume $\gamma = 1$ with g standing for the initial-time data, which for the moment is assumed to be smooth.

The inviscid Burgers PDE can be derived by considering a fluid of noninteracting particles, where at the point $x \in \mathbb{R}$ at time t the velocity of the particles is $u(x,t)$ [14, 80]. In time, despite the velocity of each particle not changing, the particles move, so the convective derivative of u vanishes,

$$0 = \frac{Du}{Dt} = \frac{\partial u}{\partial t} + u\frac{\partial u}{\partial x}. \tag{4.2}$$

4.1.1 The method of characteristics

A standard approach towards solving (4.1), is the method of characteristics.

More specifically, let γ be a smooth curve such that,

$$\gamma := \vec{c}(s) = (x(s), t(s)) \tag{4.3}$$

and

$$z(s) = u(\vec{c}(s)), \tag{4.4}$$

give the values of u along the curve γ. Then, chain differentiation leads to,

$$\frac{dz(s)}{ds} = \frac{du(x(s), t(s))}{ds} = u_x \frac{dx}{ds} + u_t \frac{dt}{ds}. \tag{4.5}$$

Setting,

$$\begin{cases} \dfrac{dt}{ds} = 1, \\ \\ \dfrac{dx}{ds} = u \end{cases} \tag{4.6}$$

leads to,

$$\frac{dx}{dt} = u. \tag{4.7}$$

Then,

$$\frac{dz}{ds} = 0 \Leftrightarrow u(x(t), t) = C. \tag{4.8}$$

The set of equation ((4.6), (4.8)) represents the characteristic equations of the respected PDE. Now, (4.8), for $t = 0$ and $x(0) = r$, gives,

$$u(x(0), 0) = C \Leftrightarrow u(r, 0) = C \Leftrightarrow g(r) = C. \tag{4.9}$$

Substituting (4.9) into (4.7), provides with,

$$x = g(r)t + D. \tag{4.10}$$

The above are straight lines passing from the point $(r, 0)$, implying that $D = r$, leading to,

$$x = g(r)t + r. \tag{4.11}$$

Now, (4.11) defines $r = r(x, t)$ implicitly as a function of x and t. Therefore, regarding u, it holds,

$$u(x, t) = u(r, 0) = g(r). \tag{4.12}$$

Differentiating (4.11) with respect to x and t, provides with,

$$\begin{cases} 1 = (1 + tg'(r))\dfrac{\partial r}{\partial x}, \\ 0 = g(r) + (1 + tg'(r))\dfrac{\partial r}{\partial t}. \end{cases} \tag{4.13}$$

Again, differentiating (4.12) with respect to x and t, gives,

$$\begin{cases} \dfrac{\partial u}{\partial x} = g'(r)\dfrac{\partial r}{\partial x}, \\ \\ \dfrac{\partial u}{\partial t} = g'(r)\dfrac{\partial r}{\partial t}. \end{cases} \tag{4.14}$$

Eliminating r_x and r_t from the above expressions, yields,

$$\begin{cases} \dfrac{\partial u}{\partial x} = \dfrac{g'(r)}{1+tg'(r)}, \\ \\ \dfrac{\partial u}{\partial t} = -\dfrac{g'(r)g(r)}{1+tg'(r)}. \end{cases} \tag{4.15}$$

Clearly, (4.1) is satisfied only if,

$$1 + tg'(r) \neq 0. \tag{4.16}$$

Summarizing, the following Theorem is established.

Theorem 1. *(Existence and Uniqueness for the inviscid Burgers initial-value problem (IVP)) [36]*

The nonlinear IVP,

$$\begin{cases} u_t + \left(\frac{u^2}{2}\right)_x = 0, \quad u = u(x,t) \in \mathbb{R}, \quad (x,t) \in \mathbb{R} \times (0,\infty), \\ u(x,0) = g(x), \quad (x,t) \in \mathbb{R} \times \{t = 0\}, \end{cases} \tag{4.17}$$

admits a unique solution assuming g is a $\mathbb{C}^1$ initial-data function, satisfying,

$$1 + tg'(r) \neq 0. \tag{4.18}$$

The solution is given in the parametric form,

$$\begin{cases} u(x,t) = g(r), \\ x = g(r)t + r. \end{cases} \tag{4.19}$$

4.1.2 Breaking time

As was previously seen, the solution $u(x,t)$ of (4.1) exists, provided (4.18) holds. Notice that this is always the case for smooth initial data and sufficiently small time t. As observed from (4.15), the spatial and time derivatives

of u tend to infinity as $1 + tg'(r) \to 0$, forcing the solution to develop a singularity when $1 + tg'(r) = 0$. Let $(x, t) = (r, 0)$ having (4.18) satisfied on the characteristics through this point, at a time t such that,

$$t = -\frac{1}{g'(r)}. \tag{4.20}$$

Notice that the latter is positive, provided $g'(r) < 0$. Hence, the solution ceases to globally exist in time in case the initial data leads to $g'(r) < 0$ for some value of r.

Definition 3. *[36] The (earliest) breaking time is defined as,*

$$t^* = min\left\{-\frac{1}{g'(x)}\right\}, \quad g'(x) < 0. \tag{4.21}$$

It is instructive to compare the solution, (4.19), of the quasilinear PDE in (4.1) with the solution,

$$u(x, t) = g(x - ct), \tag{4.22}$$

of the transport equation,

$$\begin{cases} u_t + cu_x = 0, \quad u = u(x, t) \in \mathbb{R}, \quad (x, t) \in \mathbb{R} \times (0, \infty), \\ u(x, 0) = g(x), \quad (x, t) \in \mathbb{R} \times \{t = 0\}. \end{cases} \tag{4.23}$$

In the (x, t) plane, the solution represents a propagating wave of velocity c, and $u(x, t)$ defines the wave profile at time t.

However, in the quasilinear case, the propagating speed's dependance on u, forces different parts of the wave to move with different speeds, leading towards distortion. This distortion is responsible for the solution's nonuniqueness in the quasilinear case.

A physical example, where distortion is observed, is found in the theory of shallow water waves, where the propagating speed is proportional to the square root of the depth. Its effect is that the wave's crest propagates faster than its trough, leading to wave breaking near the shore line [22, 34].

4.1.3 Self-similar solutions

Consider the equation,

$$u_t + uu_x = 0, \quad u = u(x, t), \quad (x, t) \in \mathbb{R} \times (0, \infty). \tag{4.24}$$

Under a uniform dilatation of space and time, (4.24) becomes,

$$(x,t) \mapsto (\kappa x, \kappa t), \tag{4.25}$$

providing with,

$$\kappa u_t + u\,(\kappa u_x) = \kappa\,(u_t + u u_x) = 0. \tag{4.26}$$

The latter implies an invariance under (4.25). Now, the equation under study reads,

$$mf(h) + nhf'(h) + t^{m+n+1} f(h) f'(h) = 0, \tag{4.27}$$

reducing to an ODE provided,

$$m + n + 1 = 0. \tag{4.28}$$

Due to the problem being invariant under (4.25), a natural scaling consists of $m = 0$ and $n = -1$. For the above m and n, one gets,

$$(f(h) - h) f'(h) = 0, \tag{4.29}$$

possessing the nontrivial solution,

$$f(h) = h. \tag{4.30}$$

Therefore, the self-similar solution to (4.24) is,

$$u(x,t) = \frac{x}{t}. \tag{4.31}$$

The latter is a rarefaction wave, and shall be further analyzed in the process.

4.2 Weak solution formulation

Consider the first-order, quasilinear Cauchy problem for scalar conservative forms in one space dimension,

$$\begin{cases} u_t + F(u)_x = 0 \quad \text{in} \quad \mathbb{R} \times (0,\infty), \\ u = g \quad \text{on} \quad \mathbb{R} \times \{t = 0\}. \end{cases} \tag{4.32}$$

Here, $F, g : \mathbb{R} \to \mathbb{R}$ are given and $u : \mathbb{R} \times [0,\infty) \to \mathbb{R}$ is the unknown function, $u = u(x,t)$.

The case where $F(u) = \frac{u^2}{2}$ reduces (4.32) to the inviscid Burgers PDE (4.1). The method of characteristics may produce localized in time solutions

of (4.32), due to a possible crossing of the characteristic lines. Therefore, one should devise a way of interpreting a less regular function u to somehow "solve" (4.32), beyond a possible breaking time.

Temporarily assume u to be smooth. The idea is to multiply (4.32) by a smooth function v and by applying integration by parts to transfer derivatives to v. At this stage, assume,

$$v : \mathbb{R} \times [0, \infty) \to \mathbb{R}, \quad \text{is smooth with compact support.} \tag{4.33}$$

More information can be found in the Appendix. Such a function v is called a test function. Multiply (4.32) by v and integrate by parts, using both Fubini's Theorem and the fact that v has compact support, to obtain,

$$\begin{aligned}
0 &= \int_0^\infty \int_{-\infty}^\infty [u_t + F(u)_x]v \; dxdt \\
&= \int_{-\infty}^\infty \int_0^\infty u_t v \; dtdx + \int_0^\infty \int_{-\infty}^\infty F(u)_x v \; dxdt \\
&= \int_{-\infty}^\infty \left(uv\Big|_{t=0}^{t=\infty} - \int_0^\infty uv_t \; dt \right) dx + \int_0^\infty \left(F(u)v\Big|_{x=-\infty}^{x=\infty} - \int_{-\infty}^\infty F(u)v_x \; dx \right) dt \\
&= -\int_{-\infty}^\infty u(x,0)v(x,0) \; dx - \int_0^\infty \int_{-\infty}^\infty [uv_t + F(u)v_x] \; dxdt.
\end{aligned}$$

In view of the initial condition $u = g$ on $\mathbb{R} \times \{t = 0\}$, one thereby obtains the identity,

$$\int_0^\infty \int_{-\infty}^\infty [uv_t + F(u)v_x] \; dxdt + \int_{-\infty}^\infty g(x)v(x,0) \; dx = 0, \tag{4.34}$$

for all test functions $v \in C_c^\infty(\mathbb{R} \times [0, \infty))$ [36].

The above equality was derived with u assumed to be a smooth solution of (4.32), yet the resulting formula, (4.34), has meaning even if u is only bounded. However, the above reasoning shows that a strong solution for (4.32) is always a weak solution, as well.

Definition 4. *[36] A function $u \in \mathbb{L}^\infty(\mathbb{R} \times (0, \infty))$ is an integral solution of* (4.32)*, provided* (4.34) *holds for each test function v satisfying* (4.33)*.*

The obtained integral solution of (4.32), allows for only specific types of discontinuity. Consider u as a weak solution of (4.32), being discontinuous across $x = \xi(t)$, yet both u and its first derivatives being uniformly continuous on

everywhere else. Notice that on either side of the suggested curve, everything behaves well, meaning the weak solution there is a strong solution, since it is differentiable there. Therefore, (4.34) leads back to (4.32).

Let $u^-(x,t)$ and $u^+(x,t)$ denote the limits as u approaches (x,t) from the left and the right, respectively.

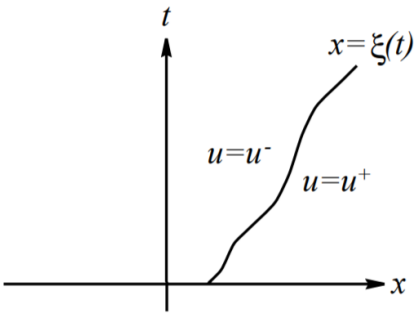

Figure 4.1: The aforementioned state for $u(x,t)$.

Theorem 2. *(Rankine–Hugoniot condition) [3, 36, 82]*

Let u be a weak solution of (4.32), being discontinuous across the curve $x = \xi(t)$, yet both u and its first derivatives are uniformly continuous on either side of $x = \xi(t)$. Then,

$$\frac{F(u^-) - F(u^+)}{u^- - u^+} = \xi'(t). \tag{4.35}$$

Proof. Assume u to be a weak solution of (4.32). Then, since (4.34) holds, choose a smooth function v with $v(x,0) = 0$ and break up the first integral of (4.34) into the sub-regions Ω^- and Ω^+ where,

$$\begin{cases} \Omega^- := \{(x,t) : 0 < t < \infty,\ -\infty < x < \xi(t)\}, \\ \Omega^+ := \{(x,t) : 0 < t < \infty,\ \xi(t) < x < \infty\} \end{cases} \tag{4.36}$$

Therefore,

$$\begin{aligned} 0 &= \int_0^\infty \int_{-\infty}^\infty [uv_t + F(u)v_x]\ dxdt + \int_{-\infty}^\infty g(x)v(x,0)\ dx \\ &= \int\int_{\Omega^-} [uv_t + F(u)v_x]\ dxdt + \int\int_{\Omega^+} [uv_t + F(u)v_x]\ dxdt. \end{aligned} \tag{4.37}$$

Utilizing the Divergence Theorem, using that v is a test function with $v(x,0) = 0$, gives,

$$\int\int_{\Omega^-} [uv_t + F(u)v_x]\, dxdt = -\int\int_{\Omega^-} [u_t + F(u)_x]v\, dxdt + \int_{x=\xi(t)} [u^- v\nu_2 + F(u^-)v\nu_1]\, ds \tag{4.38}$$

where $\nu = (\nu_1, \nu_2)$ is the outward unit normal to Ω^-. Similarly,

$$\int\int_{\Omega^+} [uv_t + F(u)v_x]\, dxdt = -\int\int_{\Omega^+} [u_t + F(u)_x]v\, dxdt - \int_{x=\xi(t)} [u^+ v\nu_2 + F(u^+)v\nu_1]\, ds. \tag{4.39}$$

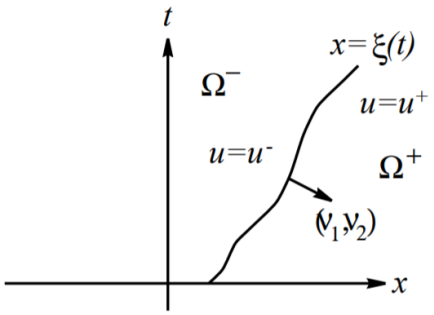

Figure 4.2: The discontinuity curve $\xi(t)$ and its outward pointing normal ν.

Now, by assumption, u is a weak solution of (4.32) with both u and its first derivatives being uniformly continuous on either side of the curve of discontinuity. Thus, u is a strong solution there. Consequently,

$$\int\int_{\Omega^-} [u_t + F(u)_x]v\ dxdt = 0 = \int\int_{\Omega^+} [u_t + F(u)_x]v\ dxdt. \tag{4.40}$$

Combining this fact with (4.37), (4.38) and (4.39), provides with,

$$\int_{x=\xi(t)} [u^- v\nu_2 + F(u^-)v\nu_1]\ ds - \int_{x=\xi(t)} [u^+ v\nu_2 + F(u^+)v\nu_1]\ ds = 0. \tag{4.41}$$

Since (4.41) holds for all test functions v, the Fundamental Lemma of Variational Calculus [42] provides with,

$$u^- v\nu_2 + F(u^-)v\nu_1 = u^+ v\nu_2 + F(u^+)v\nu_1 \tag{4.42}$$

implying that,

$$\frac{F(u^-) - F(u^+)}{u^- - u^+} = -\frac{\nu_2}{\nu_1}. \tag{4.43}$$

Regarding the slope of the curve $x = \xi(t)$, one obtains,

$$\frac{dt}{dx} = \frac{1}{\xi'(t)} = -\frac{\nu_1}{\nu_2}, \tag{4.44}$$

finally leading to,

$$\xi'(t) = -\frac{\nu_2}{\nu_1} = \frac{F(u^-) - F(u^+)}{u^- - u^+}. \tag{4.45}$$

□

Definition 5. *[36] The condition* (4.35) *is called the Rankine–Hugoniot condition along the shock curve* $x = \xi(t)$.

Set,

$$\begin{cases} [u] = u^- - u^+, \\ [F(u)] = F[u^-] - F[u^+], \\ \sigma = \xi'(t). \end{cases} \tag{4.46}$$

In that case, (4.35) is equivalently rewritten as,

$$\sigma = \frac{[F(u)]}{[u]}. \tag{4.47}$$

Remark 9. *Observe that the speed* σ *and the values* u^-, u^+, $F(u^-)$ *and* $F(u^+)$ *will generally vary along the shock curve. Despite any changes to these quantities, the expressions* $\sigma[u]$ *and* $[F(u)]$ *will always exactly balance, obeying the Rankine–Hugoniot condition.*

4.2.1 Whitham's equal-area principle

Focus is now shifted towards the fitting of shocks, obeying the Rankine–Hugoniot condition, into the continuous solution (4.19). The previous considerations demand substituting the multivalued part by a proper discontinuity. Now, the rising question is on how to correctly place this discontinuous curve.

The answer comes through a rather ingenious idea. Both the discontinuity and the multivalued curve satisfy conservation, implying that the area of u under each curve remains the same. Therefore, the shock curve should be placed in such a way that it cuts off equal areas.

The latter is known as the equal-area principle [74, 97].

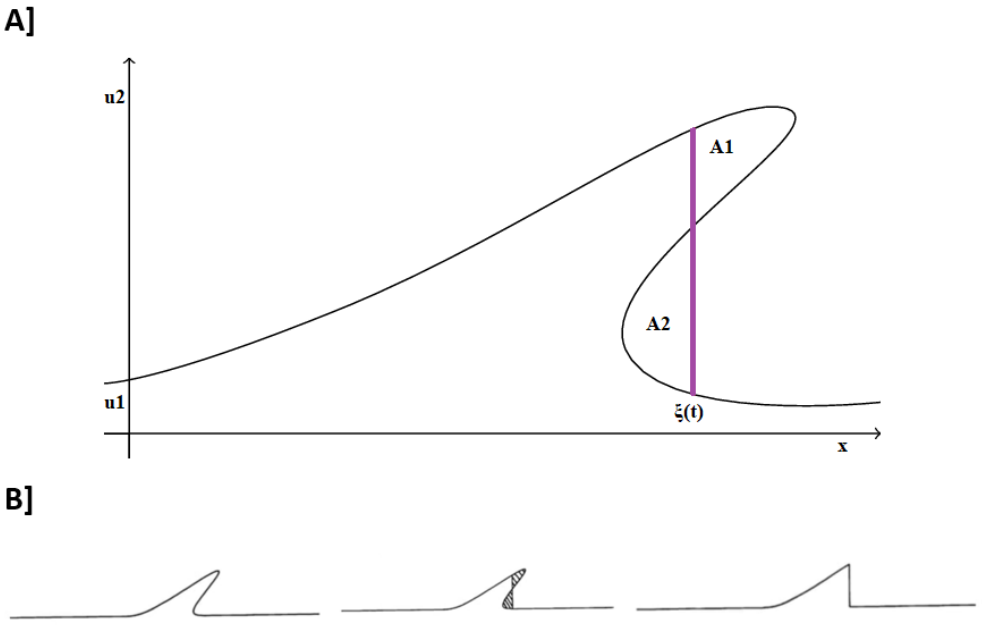

Figure 4.3: [A] Application of the equal-area principle. The shock curve is positioned in a way that $A1{=}A2$. [B] The stages of shock formation through the equal-area approach.

4.2.2 Shock wave solutions

Consider Burgers PDE, (4.1), with the initial condition,

$$g(x) = \begin{cases} 1, & x \leq 0, \\ 1 - x, & 0 \leq x \leq 1, \\ 0, & x \geq 1. \end{cases} \tag{4.48}$$

Analysis of the characteristic equations is performed as before, providing with,

$$u(x,t) = \begin{cases} 1, & x \leq t, \quad 0 \leq t \leq 1, \\ \dfrac{1-x}{1-t}, & t \leq x \leq 1, \quad 0 \leq t \leq 1, \\ 0, & x \geq 1, \quad 0 \leq t \leq 1. \end{cases} \tag{4.49}$$

However, notice the curves intersecting at $t = 1$. Thus, there's no point in seeking strong solutions, instead it's urgent seeking for a weak solution of (4.1) obeying (4.48), for $t \geq 1$.

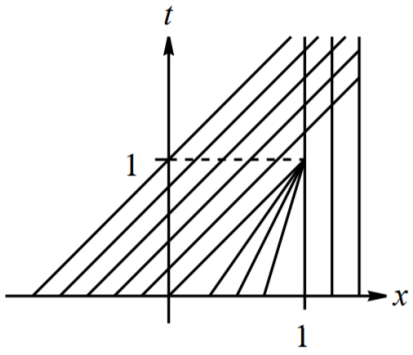

Figure 4.4: The related, crossing, characteristic curves.

For $x < 0$ and $x > 1$ one gets $u = 1$ and $u = 0$, respectively, for $t \geq 1$. Define $x = \xi(t)$ such that $u^-(x,t)$=1 and $u^+(x,t)$=0. Satisfying the Rankine–Hugoniot condition, implies,

$$\xi'(t) = \frac{1}{2}. \tag{4.50}$$

The point (1,1) belonging to $x = \xi(t)$, specifies the curve, as,

$$x - 1 = \frac{t-1}{2} \quad \Leftrightarrow \quad x = \frac{t+1}{2}. \tag{4.51}$$

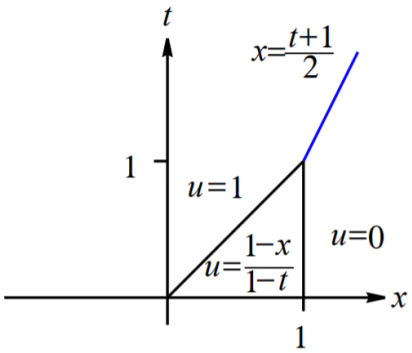

Figure 4.5: Application of the Rankine–Hugoniot condition for u(x,t)

Therefore, for $t \geq 1$ let,

$$u(x,t) = \begin{cases} 1, & x < \frac{t+1}{2}, \\ 0, & x > \frac{t+1}{2}. \end{cases} \tag{4.52}$$

Summarizing, the solution of ((4.1), (4.48)) is given by (4.49) for $t \leq 1$ and (4.52) for $t \geq 1$.

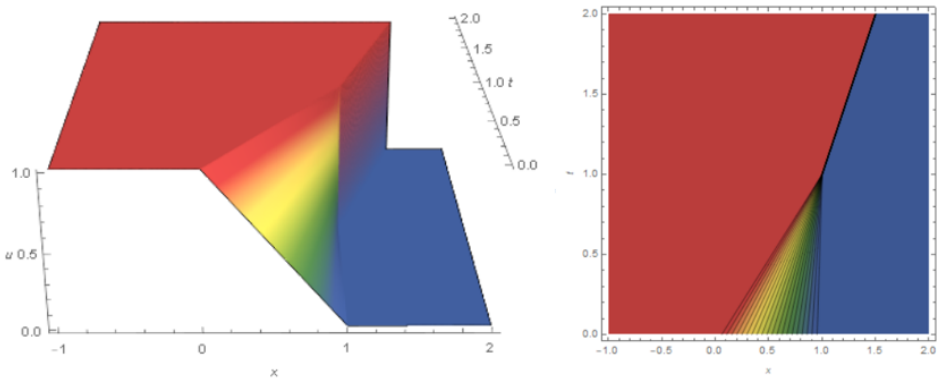

Figure 4.6: The shock solution $u(x,t)$.

Remark 10. *A shock either extends infinitely or together with a second shock form a third [74].*

4.2.3 Rarefaction wave solutions

Consider Burgers PDE (4.1), this time with the initial condition,

$$g(x) = \begin{cases} 0, & x < 0, \\ 1, & x > 0. \end{cases} \tag{4.53}$$

Studying the characteristics, one deduces that no crossing occurs. However, what's interesting here is dealing with a region on which there's not enough information.

One possible way of filling the region of information loss is by mimicing previous work, letting,

$$u_1(x,t) = \begin{cases} 0, & x < \frac{t}{2}, \\ 1, & x > \frac{t}{2}. \end{cases} \tag{4.54}$$

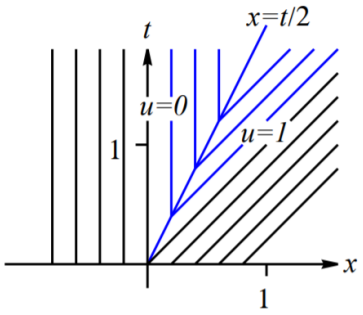

Figure 4.7: u_1 as a possible and allowed filling of the information gap.

A second candidate is,

$$u_2(x,t) = \begin{cases} 0, & x \leq 0, \\ \dfrac{x}{t}, & 0 \leq x \leq t, \\ 1, & x \geq t. \end{cases} \tag{4.55}$$

Notice that $u_2(x,t)$ is a continuous solution of (4.1), satisfying (4.53).

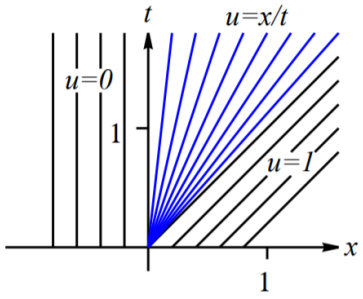

Figure 4.8: u_2 as an other possible and allowed filling of the information gap.

Concluding, two different solutions are found. Is it possible, however, that one solution is more physically realistic than the other, and if so, how to distinguish the two solutions? The answer is found later on, where the notion of an entropy condition is discussed. The solution u_2, as it's about to be described, obeys the entropy condition.

Definition 6. *[36] A wave, "fanning" the wedge* $0 < x < t$*, is called a rarefaction wave.*

More information can be found in the Appendix.

4.2.4 An example of both shock and rarefaction

In the view of obtaining solutions of both shock and rarefaction characteristics, deal with the Cauchy problem (4.1), with g satisfying,

$$g(x) = \begin{cases} 1, & 0 < x < 1, \\ 0, & \text{elsewhere} \end{cases} \tag{4.56}$$

Again, the characteristic equations are derived as before, indicating an occuring rarefaction wave between $x = 0$ and $x = t$, as well as a formed shock, due to the intersection of the lines $x = t + r$, for $0 < r < 1$, and $x = 1$.

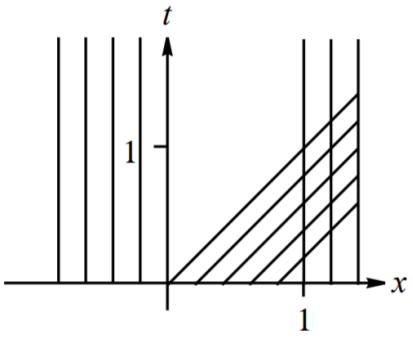

Figure 4.9: The related, crossing, characteristic curves, revealing a region of information loss.

Because of the Rankine–Hugoniot condition, the shock speed σ equals to $\frac{1}{2}$, implying that the shock curve emanating from $(1, 0)$ is $x = 1 + \frac{t}{2}$.

However, focusing at $t = 2$, the rarefaction wave meets the shock curve. Demand the jump along the shock to obey the Rankine–Hugoniot condition. Notice that $u^- = \frac{x}{t}$ and $u^+ = 0$ hold to the left and right of the jump, respectively.

The Rankine–Hugoniot condition reads,

$$\sigma = \frac{\frac{1}{2}\left(\frac{x}{t}\right)^2 - 0}{\left(\frac{x}{t}\right) - 0} = \frac{x}{2t}. \tag{4.57}$$

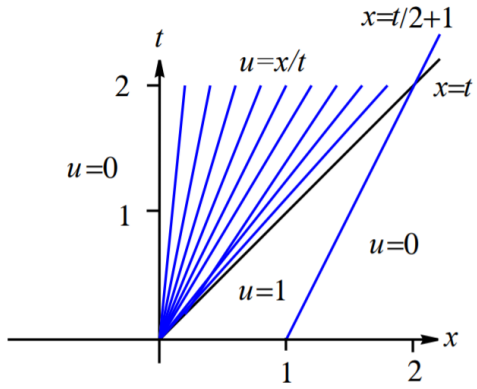

Figure 4.10: The proper, entropy-respecting, filling of the information gap.

Asking for the point $(2, 2)$ to belong to the obtained curve, leads to $x(t) = \sqrt{2t}$.

In summary,

$$u(x,t) = \begin{cases} 0, & x < 0, \\ \dfrac{x}{t}, & 0 < x < t, \\ 1, & t < x < 1 + \dfrac{t}{2}, \\ 0, & x > 1 + \dfrac{t}{2} \end{cases} \qquad t \leq 2 \tag{4.58}$$

and

$$u(x,t) = \begin{cases} 0, & x < 0, \\ \dfrac{x}{t} & 0 < x < \sqrt{2t}, \\ 0, & x > \sqrt{2t} \end{cases} \qquad t \geq 2 \tag{4.59}$$

Notice that $|u| \to 0$ as t tends to infinity. More precisely, using the solution formula derived above, observe that,

$$\begin{cases} |u(x,t)| \leq 1, & 0 \leq t \leq 2, \\ |u(x,t)| \leq \dfrac{x}{t} \leq \dfrac{\sqrt{2t}}{t} = \dfrac{\sqrt{2}}{\sqrt{t}}, & t \geq 2, \end{cases} \tag{4.60}$$

implying that,

$$|u(x,t)| \leq \frac{\sqrt{2}}{\sqrt{t}}, \quad \text{for any} \quad t > 0, \quad x \in \mathbb{R}. \tag{4.61}$$

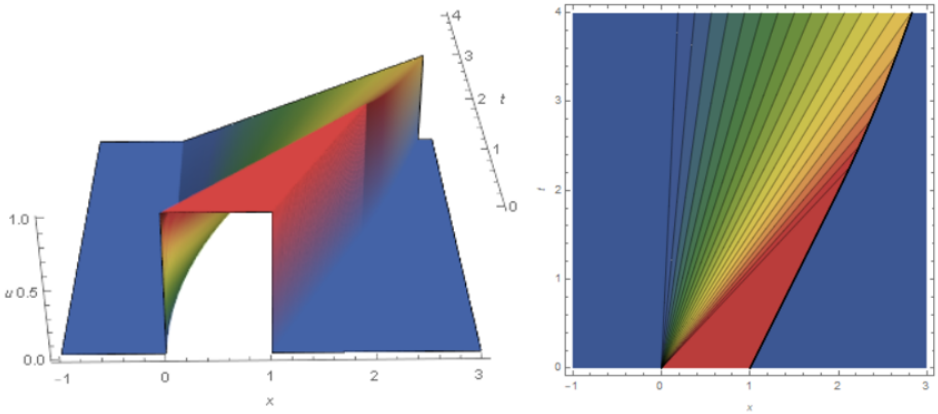

Figure 4.11: The solution $u(x,t)$, showing both shock and rarefaction wave characteristics.

Remark 11. *The latter shows that u vanishes like $\dfrac{1}{\sqrt{t}}$ as t gets arbitrary large. This key-property is thoroughly analyzed later on.*

4.2.5 The entropy condition

As was previously seen, integral solutions are generally not unique. The current purpose is finding a criterion ensuring uniqueness.

In this matter, consider the conservative form (4.32), equivalently written as,

$$u_t + F'(u)u_x = 0. \tag{4.62}$$

The characteristic equations, associated with (4.62), are given by,

$$\begin{cases} \dfrac{dt}{ds} = 1, \\ \dfrac{dx}{ds} = F'(z), \\ \dfrac{dz}{ds} = 0. \end{cases} \tag{4.63}$$

Deduce that the speed of u, $\dfrac{du}{dt}$ is,

$$\frac{du}{dt} = F'(u). \tag{4.64}$$

Particularly, for Burgers equation,

$$\frac{du}{dt} = u, \tag{4.65}$$

pointing to taller waves propagating faster compared to the shorter. As a result, in ((4.1), (4.48)) it's expected that the left part of the wave overtakes the right, resulting to the curve of discontinuity. However, in ((4.1), (4.53)), the wave is higher to the right. Consequently, the right part of the wave is expected to move faster.

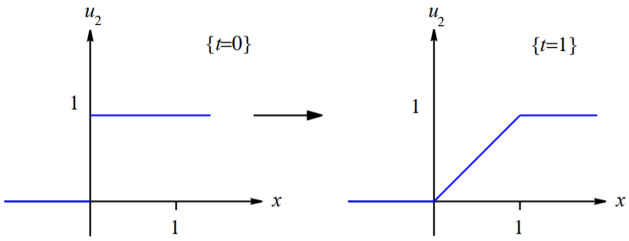

Figure 4.12: Time evolution of $u_2(x,t)$.

Now, let's make these ideas more precise. A discontinuous curve between u^- and u^+ is only allowed if,

$$F'(u^-) > \sigma > F'(u^+). \tag{4.66}$$

Definition 7. *[36] Condition* (4.66) *is called the entropy condition, from a rough analogy with the thermodynamic principle stating that entropy cannot decrease as time goes forward.*

Definition 8. *[36] A discontinuous curve is called a shock curve for a solution u, when it satisfies both the Rankine–Hugoniot and entropy condition for u.*

Therefore, the only admissible solutions u, are the ones for which curves of discontinuity are shock curves. The latter is stated more precisely as follows.

Remark 12. *Physical phenomena, mathematically modeled by continuous solutions of a quasilinear hyperbolic system, are reversible in time. However, that's not the case for those described by shock discontinuities.*

Consider the Cauchy problem,

$$\begin{cases} u_t + F(u)_x = 0 \quad \text{in} \quad \mathbb{R} \times (0, \infty), \\ u = g \quad \text{on} \quad \mathbb{R} \times \{t = 0\}. \end{cases} \tag{4.67}$$

Definition 9. *[36] A function u is a weak, admissible solution of* (4.67)*, provided u is a weak solution admitting only shock curves.*

In ((4.1), (4.53)), possibility one, for,

$$\begin{cases} u^- = 0, \\ u^+ = 1, \\ \sigma = \xi'(t) = \dfrac{1}{2}, \end{cases} \tag{4.68}$$

gave,

$$F'(u^-) = u^- = 0 \leq \frac{1}{2} \leq 1 = u^+ = F'(u^+). \tag{4.69}$$

The latter implies that u_1 isn't admissible, whereas u_2 is a continuous solution, admitting no curves of discontinuity. Therefore, it satisfies the entropy condition, and it's physically accepted.

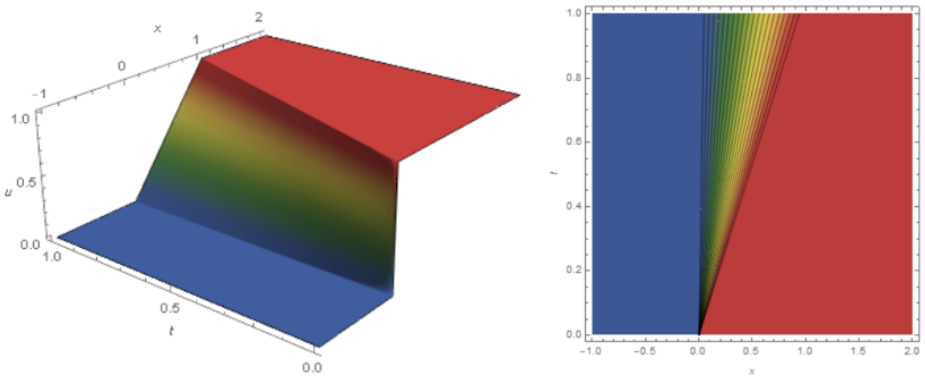

Figure 4.13: The rarefaction wave solution $u_2(x, t)$.

The focus is now shifted to Cauchy problems of the form (4.67) with F possessing a particular structure.

Definition 10. *[36] A function F is called uniformly convex if,*

$$F'' \geq \theta > 0 \quad \textit{for} \quad \theta > 0. \tag{4.70}$$

More specifically, this points to F' being strictly increasing. For a strictly increasing F', u obeys the entropy condition (4.66) iff,

$$u^- > u^+, \tag{4.71}$$

on any curve of discontinuity.

Therefore, u will be a weak, admissible solution to,

$$u_t + F(u)_x = 0, \tag{4.72}$$

iff u meets the Rankine–Hugoniot condition, as well as,

$$u^- > u^+, \tag{4.73}$$

along any curves of discontinuity. It's now worth mentioning the main uniqueness result, whose detailed proof can be found in Evans §3.4.3b [36].

Theorem 3. *(Uniqueness of entropy solutions) [36]*

Assume F is convex and smooth. Then, there exists, up to a set of measure zero, at most one entropy solution of (4.67).

4.2.6 Riemann's problem

Moving further, in this section, consider the Cauchy problem,

$$\begin{cases} u_t + F(u)_x = 0 \quad t \geq 0 \\ u(x,0) = g(x) \end{cases} \tag{4.74}$$

with F being uniformly convex and g piecewise constant,

$$g(x) = \begin{cases} u^-, & x < 0 \\ u^+, & x > 0 \end{cases} \tag{4.75}$$

Definition 11. *[36] The above problem is known as Riemann's problem for* (4.74). *The constants u^- and u^+ denote the left and right initial states, with $u^- \neq u^+$. F is still assumed being uniformly convex C^2 with $G = (F')^{-1}$.*

Theorem 4. *[36]*

1. *In the case of $u^- > u^+$, the admissible solution has a shock curve of speed σ and is given by,*

$$u(x,t) = \begin{cases} u^-, & \frac{x}{t} < \sigma \\ u^+, & \frac{x}{t} > \sigma \end{cases} \quad , \quad \sigma = \frac{[F(u)]}{[u]} \tag{4.76}$$

2. *In the case of* $u^- < u^+$*, the solution has a rarefaction wave and is given by,*

$$u(x,t) = \begin{cases} u^-, & \frac{x}{t} < F'(u^-) \\ G\left(\frac{x}{t}\right), & F'(u^-) < \frac{x}{t} < F'(u^+) \\ u^+, & \frac{x}{t} > F'(u^+) \end{cases} \quad , \quad G = (F')^{-1} \tag{4.77}$$

Proof. Initially, one deals with Case 1. Clearly, by differentiation and substitution, $u(x,t)$ defined in (4.76) is a strong solution of ((4.74),(4.75)), on either side of the curve $x = \sigma t$. Additionally, the curve of discontinuity satisfies the Rankine–Hugoniot jump condition, implying that $u(x,t)$ is a weak solution. Moreover, as hypothesized, $u^- > u^+$ and F is uniformly convex, with,

$$F'(u^+) < \sigma := \frac{[F(u)]}{[u]} = \frac{F(u^-) - F(u^+)}{u^- - u^+} = \frac{1}{u^- - u^+} \int_{u^+}^{u^-} F'(r)\, dr < F'(u^-) \tag{4.78}$$

Therefore, u satisfies the entropy condition. Uniqueness shall follow from Theorem (3). Now, look at Case 2. For u defined by (4.77), u is a strong solution of ((4.74), (4.75)) to the left of $x = F'(u^-)t$ and to the right of $x = F'(u^+)t$. Thus, one is left with checking if u is also a solution for $F'(u^-) < \frac{x}{t} < F'(u^+)$.

Using the Chain Rule,

$$\begin{aligned} u_t + F(u)_x &= G'\left(\frac{x}{t}\right)\left(-\frac{x}{t^2}\right) + F'\left(G\left(\frac{x}{t}\right)\right) G\left(\frac{x}{t}\right)_x \\ &= G'\left(\frac{x}{t}\right)\left(-\frac{x}{t^2}\right) + F'\left((F')^{-1}\left(\frac{x}{t}\right)\right) G'\left(\frac{x}{t}\right)\left(\frac{1}{t}\right) \\ &= G'\left(\frac{x}{t}\right)\left(-\frac{x}{t^2}\right) + G'\left(\frac{x}{t}\right)\left(\frac{x}{t^2}\right) \\ &= 0 \end{aligned}$$

Therefore, u is a strong solution in each of the three regions in which it is defined. Furthermore, along the curve $\frac{x}{t} = F'(u^-)$, the fact that,

$$G\left(\frac{x}{t}\right) = (F')^{-1}\left(\frac{x}{t}\right) = u^- \tag{4.79}$$

implies that $u(x,t)$ is continuous across the curve $\frac{x}{t} = F'(u^-)$. In a similar manner, $u(x,t)$, as defined in (4.77), is also continuous across the curve $\frac{x}{t} = F'(u^+)$.

Therefore, u satisfies the entropy condition. Notice that u also satisfies (4.34).

Finally, one may as well assume that G is Lipschitz continuous, satisfying,

$$u(x+z,t) - u(x,t) = G\left(\frac{x+z}{t}\right) - G\left(\frac{x}{t}\right) \leq \frac{Lip(G)}{t} z \tag{4.80}$$

with,

$$F'(u^-)t < x < x+z < F'(u^+)t. \tag{4.81}$$

The latter inequality implies that u obeys the entropy condition, enabling one to again ensure uniqueness from Theorem (3). □

A crucial point when handling conservative forms is when transforming the original form to a seemingly equivalent one. In this case, although any smooth solutions of the two are in general equivalent, the same result doesn't hold for the respected weak solutions. A convincing justification comes through multiplying both sides of the inviscid Burgers equation by $2u$, obtaining the seemingly equivalent conservative form,

$$\left(u^2\right)_t + \left(\frac{2}{3}u^3\right)_x = 0. \tag{4.82}$$

The two above equations admit the same smooth solutions. However, consideration of the Riemann problem for $u^- > u^+$, provides with,

$$\begin{cases} \sigma_1 = \dfrac{\left[\dfrac{1}{2}u^2\right]}{[u]} = \dfrac{1}{2}\left(u^- + u^+\right), \\ \\ \sigma_2 = \dfrac{\left[\dfrac{2}{3}u^3\right]}{[u^2]} = \dfrac{2}{3}\left(\dfrac{(u^-)^3 - (u^+)^3}{(u^-)^2 - (u^+)^2}\right) \end{cases} \tag{4.83}$$

Notice that,

$$\sigma_2 - \sigma_1 = \frac{1}{6}\frac{\left(u^- - u^+\right)^2}{u^- + u^+} \neq 0 \tag{4.84}$$

implying that the respected weak solutions shall differ.

4.2.7 Long-time asymptotics

Consider the most general conservative form, (4.32), under the following assumptions.

1. $g(x)$ is a bounded and integrable initial-data function.

2. F is smooth and uniformly convex, such that $F(0) = 0$.

The following result demonstrates the qualitative way $|u|$ vanishes as time gets sufficiently large.

Theorem 5. *(Asymptotics in $\mathbb{L}^\infty$ norm) [36]*

Consider a Cauchy problem of the form of (4.32)*, with F and g obeying the hypothesis indicated. In this setting,*

$$|u(x,t)| \leq \frac{C}{\sqrt{t}}, \quad \textit{for all} \;\; t > 0, \quad x \in \mathbb{R}, \quad \textit{for some} \quad C > 0. \tag{4.85}$$

Proof. Start by setting,

$$\begin{cases} \sigma := F'(0), \\ G = (F')^{-1} \end{cases} \tag{4.86}$$

leading to,

$$G(\sigma) \overset{(4.86)}{=} (F')^{-1}\left(F'(0)\right) = 0 \tag{4.87}$$

In the same manner as the Hopf–Lax formula is derived [36], consider,

$$L = F^*. \tag{4.88}$$

Here, F^* denotes the Legendre (or Fenchel) transform of F [36], satisfying,

$$\begin{cases} L(\sigma) \overset{(4.88)}{=} \sigma G(\sigma) - F(G(\sigma)) \overset{(4.87)}{=} 0, \\ L'(\sigma) = 0 \end{cases} \tag{4.89}$$

At this stage, in view of both (4.89) and the uniform convexity of L, it holds,

$$\begin{aligned} tL\left(\frac{x-y}{t}\right) &= tL\left(\frac{x-y}{t}+\sigma-\sigma\right) \\ &= tL\left(\frac{x-y-\sigma t}{t}+\sigma\right) \\ &\geq t\left[L(\sigma)+L'(\sigma)\left(\frac{x-y-\sigma t}{t}\right)+\theta\left(\frac{x-y-\sigma t}{t}\right)^2\right] \\ &= \theta\frac{(x-y-\sigma t)^2}{t}, \quad \text{for some } \ \theta>0. \end{aligned} \tag{4.90}$$

Since,

$$h(y)=\int_0^x g(y)\ dy \tag{4.91}$$

is bounded by $M := ||g||_{\mathbb{L}_1}$, deduce from (4.90) that,

$$tL\left(\frac{x-y}{t}\right)+h(y) \geq \theta\frac{(x-y-\sigma t)^2}{t}-M \tag{4.92}$$

On the other hand,

$$\begin{aligned} M &\geq h(x-\sigma t) \\ &= h(x-\sigma t)+tL(\sigma), \quad (\text{since } \ L(\sigma)=0) \\ &= h(x-\sigma t)+tL\left(\frac{x-(x-\sigma t)}{t}\right). \end{aligned}$$

Therefore, at the minimizing point $y(x,t)$, it holds,

$$\begin{aligned} \theta\frac{(x-y(x,t)-\sigma t)^2}{t} = \theta\frac{|x-y(x,t)-\sigma t|^2}{t} &\leq 2M \\ \Rightarrow \theta\frac{|x-y(x,t)-\sigma t|^2}{t^2} &\leq \frac{2M}{t} \\ \Rightarrow \frac{|x-y(x,t)-\sigma t|^2}{t^2} &\leq \frac{2M}{\theta t} \\ \Rightarrow \left|\frac{x-y(x,t)-\sigma t}{t}\right|^2 &\leq \frac{2M}{\theta t} \\ \Rightarrow \left|\frac{x-y(x,t)}{t}-\sigma\right|^2 &\leq \frac{2M}{\theta t} \\ \Rightarrow \left|\frac{x-y(x,t)}{t}-\sigma\right| &\leq \frac{C}{t^{1/2}}, \quad C:=\sqrt{\frac{2M}{\theta}}>0. \end{aligned} \tag{4.93}$$

Since $G(\sigma) = 0$, for any $x \in \mathbb{R}$, $t > 0$, one finally obtains,

$$\begin{aligned} |u(x,t)| &= \left| G\left(\frac{x - y(x,t)}{t}\right) \right| \\ &= \left| G\left(\frac{x - y(x,t)}{t} + \sigma - \sigma\right) - G(\sigma) \right| \\ &\leq Lip(G) \left| \frac{x - y(x,t)}{t} - \sigma \right| \\ &\leq \frac{C}{t^{1/2}}, \quad \text{(in accordance to (4.93).} \end{aligned}$$

□

Even more specifically, solutions of (4.32), in general, can be proven to decay to an N-wave [36].

Definition 12. *[36] Given constants $p, q \geq 0$, $d > 0$ and σ, a N-wave is defined as,*

$$N(x,t) = \begin{cases} \frac{1}{d}\left(\frac{x}{t} - \sigma\right), & \text{for } -\sqrt{pdt} < x - \sigma t < \sqrt{pdt} \\ 0, & \text{elsewhere} \end{cases} \tag{4.94}$$

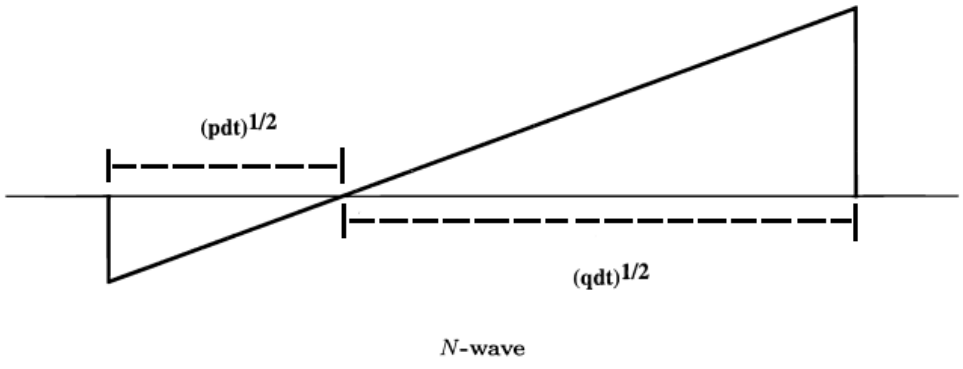

Figure 4.14: A N-wave form.

Focus is turned on a specific N-wave, given by,

$$\begin{cases} p = -2\min\limits_{y\in\mathbb{R}} \int_{-\infty}^{y} g(x)\ dx, \\ \\ q = 2\max\limits_{y\in\mathbb{R}} \int_{y}^{\infty} g(x)\ dx, \\ \\ d = F''(0) > 0, \\ \\ \sigma = F'(0), \end{cases} \tag{4.95}$$

which will be useful in introducing the following result on the shape u evolves into in $\mathbb{L}_1$. A detailed proof can be found in Evans §3.4.5b [36].

Theorem 6. *(Asymptotics in $\mathbb{L}_1$ norm) [36]*

Consider a Cauchy problem of the form (4.32) *where F is smooth and uniformly convex, g has compact support, p, q, d, and σ are defined in* (4.95) *and $N(x,t)$ is defined in* (4.94)*. In this setting,*

$$\int_{-\infty}^{\infty} |u(x,t) - N(x,t)|\ dx \leq \frac{C}{\sqrt{t}}, \quad \textit{for all} \ \ t > 0, \quad \textit{for some} \quad C > 0. \tag{4.96}$$

Now, let's use the Cauchy problem ((4.1), (4.56)) to verify that Theorem (6) holds.

Notice that, using (4.94) and (4.95), $N(x,t)$ in this case takes the form,

$$N(x,t) = \begin{cases} \dfrac{x}{t}, & \text{for} \ \ 0 < x < \sqrt{2t}, \\ 0, & \text{elsewhere} \end{cases} \tag{4.97}$$

Now, for $0 \leq t \leq 2$, one gets,

$$\begin{aligned} \int_{-\infty}^{\infty} |u(x,t) - N(x,t)|\ dx &= \int_{0}^{1+\frac{t}{2}} |u(x,t) - N(x,t)|\ dx \\ &= \int_{0}^{t} \left| \frac{x}{t} - \frac{x}{t} \right| dx + \int_{1}^{\sqrt{2t}} \left| 1 - \frac{x}{t} \right| dx + \int_{\sqrt{2t}}^{1+\frac{t}{2}} |1 - 0|\ dx \\ &\leq \frac{6\sqrt{2}}{\sqrt{t}} \end{aligned}$$

while $u(x,t) = N(x,t)$ for all $t \geq 2$.

Remark 13. *The dynamics of the Burgers equation, push any compactly supported initial data towards an N-wave.*

CHAPTER 5

Numerical and Semi-Analytical Methods

5.1 Time-evolved profiles of the KdV–B equation

Consider the KdV–B equation,

$$u_t + \gamma u u_x - \alpha u_{xx} + \beta u_{xxx} = 0. \tag{5.1}$$

Rearrangement of its terms, provides with,

$$u_t = -\gamma u u_x + \alpha u_{xx} - \beta u_{xxx}. \tag{5.2}$$

Utilizing the Fourier Transform, (5.2) can be written in the form [85],

$$\frac{\partial u}{\partial t} = f(t, u), \tag{5.3}$$

where the x-partial derivatives are substituted with,

$$\begin{cases} u_x = iF^{-1}(\kappa \hat{u}), \\ u_{xx} = -F^{-1}(\kappa^2 \hat{u}), \\ u_{xxx} = -iF^{-1}(\kappa^3 \hat{u}) \end{cases} \tag{5.4}$$

Now, (5.3) is suitable for applying the 4th order Runge–Kutta scheme. More information can be found in the Appendix.

As an initial guess, a pulse is chosen and its gradual deformation, due to time evolution, is observed.

Remark 14. *The obtained numerical solutions clearly reveal both solitary and shock wave features of the KdV–B equation, revealing its connection to cardiac hemodynamics where all these phenomena, such as convection, diffusion and dispersion, can be observed.*

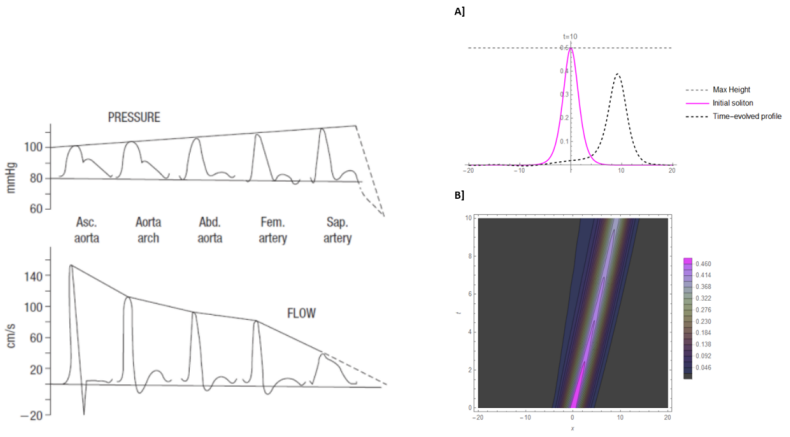

Figure 5.1: Arterial pressure and flow waveforms exhibiting similar qualitative features to a time-evolved pulse of KdV–B. The parameters chosen are, $\lambda = 1$, $\alpha = 0.1$, $\beta = 1$ and $\gamma = 6$.

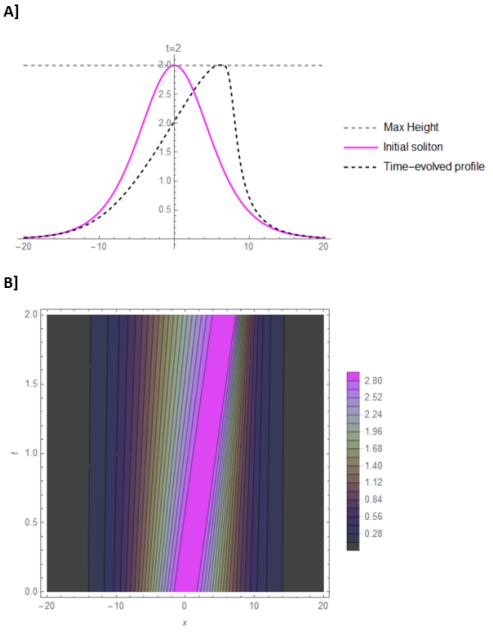

Figure 5.2: [A] A time-evolved pulse of KdV–B, with KdV–B, of both diffusive and dispersive characteristics, for $\lambda = 1$, $\alpha = 0.01$, $\beta = 0.1$, $\gamma = 1$. [B] The respected contour plot.

5.2 A Computational Spectral Fourier Approach

A computational spectral Fourier approach [2, 6, 87] is discussed. Executed in the Fourier space, the spectral scheme leads to a coupling between an algebraic system and an integral equation. A convergent fixed point iteration scheme together with the Inverse Fast Fourier Transform, finally grant the solitary wave solution.

The method is tested with an emphasis given to its applicability to fluid dynamics. Both pulse and wavefront profiles will be derived.

5.2.1 The Spectral Scheme for KP

Aiming to a spectral numerical solution of KP, instead of solving (3.53) exactly, apply the Fast Fourier Transform (FFT), being the discrete analogue of the well known Fourier Transform, getting,

$$F\left\{u'' + \frac{(3\delta^2 - \lambda)}{\beta}u + \frac{\gamma}{2\beta}u^2\right\} = 0. \tag{5.5}$$

Using well-known properties of FFT, equation (5.5) reads,

$$\hat{u} = \frac{\frac{\gamma}{2\beta}F\left\{u^2\right\} + \left(\frac{3\delta^2 - \lambda}{\beta} + R\right)\hat{u}}{\kappa^2 + R}. \tag{5.6}$$

Construction of a nontrivial and bounded solution, demands introducing v such that,

$$\begin{aligned} u &= cv \\ \Leftrightarrow \hat{u} &= c\hat{v}, \end{aligned} \tag{5.7}$$

where $c \neq 0$ is to be determined [2]. Substitution of (5.7) into (5.6), gives,

$$\hat{v} = \frac{\frac{\gamma}{2\beta}c\ F\left\{v^2\right\}}{\kappa^2 + \frac{\lambda - 3\delta^2}{\beta}}. \tag{5.8}$$

Additionally, multiplying (5.8) by $\hat{v}^*$, being the conjugate of $\hat{v}$, and integrating over the frequency domain, one obtains,

$$c = \frac{2\beta}{\gamma} \frac{\displaystyle\int_{-\infty}^{\infty} \left(\kappa^2 + \frac{\lambda - 3\delta^2}{\beta}\right) |\hat{v}|^2 d\kappa}{\displaystyle\int_{-\infty}^{\infty} F\left\{v^2\right\} \hat{v}^* d\kappa}. \tag{5.9}$$

Equations (5.8) and (5.9) provide a fixed point iteration scheme, whose solution for c and v can be expressed as,

$$\begin{cases} c_n = \dfrac{2\beta}{\gamma} \dfrac{\displaystyle\int_{-\infty}^{\infty} \left(\kappa^2 + \frac{\lambda - 3\delta^2}{\beta}\right) |\hat{v_n}|^2 d\kappa}{\displaystyle\int_{-\infty}^{\infty} F\left\{v_n^2\right\} \hat{v_n}^* d\kappa}, \\ \\ \hat{v_{n+1}} = \dfrac{\frac{\gamma}{2\beta} c \; F\left\{v_n^2\right\}}{\kappa^2 + \dfrac{\lambda - 3\delta^2}{\beta}} \end{cases} \tag{5.10}$$

When $n = 0$ an initial localized guess is required, for example a Gaussian [2, 6, 87].

Throughout the paper, regarding the initial guesses, c_0 and v_0,

$$c_0 = 1, \quad v_0(x) = \mathrm{e}^{-x^2} \tag{5.11}$$

are proposed. The spectral scheme, (5.10), is selected to be continuously iterated until,

$$\begin{cases} |c_{n+1} - c_n| \leq 10^{-10}, \\ \\ \left| F^{-1}\{\hat{v_{n+1}}\} - F^{-1}\{\hat{v_n}\} \right|_{\infty} \leq 10^{-10}, \quad n \geq 0 \end{cases} \tag{5.12}$$

are both satisfied.

Remark 15. *The spectral approach is a method of spectral accuracy, regarding the spatial variables, converging rapidly to a solution of the required accuracy [2, 6, 87].*

5.2.2 The Spectral Scheme for KdV–B

The spectral analysis has been, so far, focused on an evolution equation admitting pulse solutions, being localized wave disturbances obeying vanishing boundary conditions. However, as shown in the KdV–B case, shock wave solutions asymptotically tending to a nontrivial background state also exist.

Such solutions are of both analytical and experimental research [2, 90]. Examinination of these solutions asks for a different approach to the spectral scheme. The next remark summarizes the idea about to be followed.

Remark 16. *The main difficulty when studying wavefronts is that the non-vanishing behavior at infinity doesn't allow for transform methods to be immediately applied. To overcome this situation, spatial differentiation of the equation is performed, with the spectral approach applied to the derivative of the wavefront [2, 6]. The obtained solution is finally integrated over the spatial domain.*

Now, let's apply the aforementioned ideas to the KdV–B equation, seeking for a numerical wavefront solution. Differentiation of (2.20) with respect to x provides with,

$$u_{tx} + \gamma \left(u_x^2 + u u_{xx}\right) - \alpha u_{xxx} + \beta u_{xxxx} = 0. \tag{5.13}$$

Set

$$u_x := v(x,t), \quad v(\pm\infty, t) = 0. \tag{5.14}$$

Then, (5.13) transforms into,

$$v_t + \gamma \left(v^2 + v_x \int v \, dx\right) - \alpha v_{xx} + \beta v_{xxx} = 0. \tag{5.15}$$

The traveling wave transform, converts (5.15) into,

$$-\lambda v(\zeta) + \gamma \left(v^2(\zeta) + v'(\zeta) \int v(\zeta) \, d\zeta\right) - \alpha v''(\zeta) + \beta v'''(\zeta) = 0. \tag{5.16}$$

Now, the spectral approach is applied to (5.16). The respected scheme shall

now be,

$$\begin{cases} c_n = -\dfrac{1}{\gamma}\dfrac{\displaystyle\int_{-\infty}^{\infty}(\alpha\kappa^2 + i(\lambda\kappa + \beta\kappa^3)|\hat{v_n}|^2 d\kappa}{\displaystyle\int_{-\infty}^{\infty} F\left\{v_n^2 + v_n' \int v_n\right\}\hat{v_n}^* d\kappa}, \\ \hat{v_{n+1}} = \dfrac{-\gamma c_n F\left\{v_n^2 + v_n' \int v_n\right\} + (R - i(\lambda\kappa + \beta\kappa^3))\hat{v_n}}{\alpha\kappa^2 + R}, \quad R > 0 \end{cases} \tag{5.17}$$

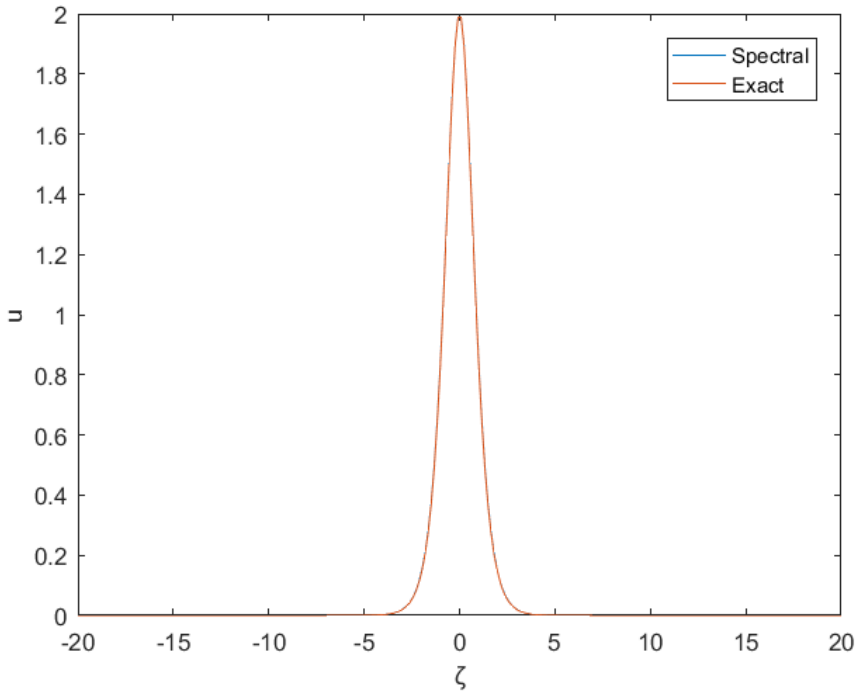

Figure 5.3: A common plot of the exact line-soliton and the spectral solution of KP, for the values of $\lambda = \beta = 1$, $\gamma = 6$, $\delta = i$ and $R = 1$, with $(x, y, t) \in [-20, 20] \times \{0\} \times \{0\}$.

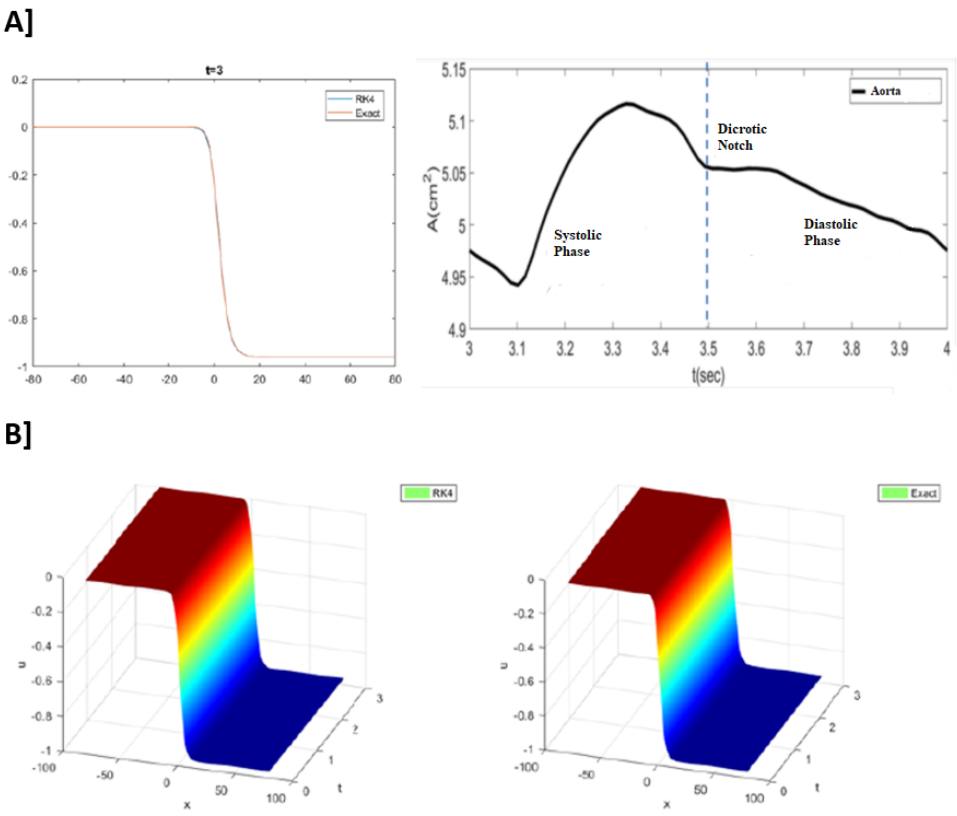

Figure 5.4: [A] The exact shock and RK4 solutions of KdV–B. Notice the resemblance with the dicrotic notch stage. [B] The RK4 solution, evolving the shock spectral solution (left), and an exact solution (right), for the values of $\alpha = \gamma = 0.01$, $\beta = 0.005$ and $R = 200$, with $(x, t) \in [-80, 80] \times [0, 3]$.

5.3 A semi-exact homotopy analysis approach

The key-idea of this section originates from the topological notion of homotopy, more information on which can be found in the Appendix.

The homotopy method is a semi-exact approach utilizing the notion of homotopy to generate a convergent series solution for nonlinear systems. A homotopy-Maclaurin series is formed to cope with the system's nonlinearities. The approach was initially devised in 1992 by Liao and further modified in 1997, utilizing the convergence-control parameter, $\hbar$, into forming a homotopy on a differential system [58]. The purpose of $\hbar$ is to verify and enforce the

method's convergence.

The homotopy approach presents with notable features. First, the derived series expansion is independent on the scale of the system's parameters. Thus, it deals with both weakly and strongly nonlinear problems, going past the standard inherent limitations of perturbation methods. Second, the method generalizes and unifies many other approaches [9, 56, 77]. Third, excellent flexibility is provided in both explicitly deriving and expressing the solution. Great freedom is given in selecting both the basis functions of the desired solution and the linear operator of the homotopy. Finally, it distinguishes itself from the other analytic approximation methods, in granting the convergence of the solution series [58].

Recently, the method has efficiently dealt with nonlinear systems [59, 73, 88, 100]. Phenomena in deep and finite water depth [60, 101], nonlinear dynamic systems [23], the exact Navier–Stokes equation [86], boundary layer equations [73, 100], as well as the Whitham–Broer–Kaup model [75], have all been efficiently studied by the homotopy method. It's worth emphasizing that the homotopy method combines well with spectral methods and Pade approximants [69].

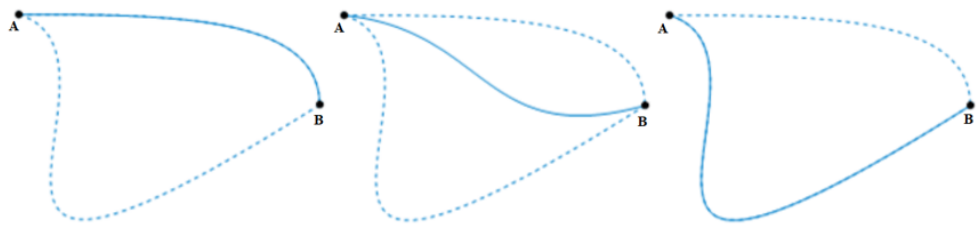

Figure 5.5: A homotopy between two homotopic dashed paths.

5.3.1 The homotopy method for the KdV–B equation

In this section, the homotopy method is applied to the KdV–B equation. Consider an initial wavefront profile,

$$u(x,0) = \frac{\mathrm{e}^{-x}}{1+\mathrm{e}^{-x}}. \tag{5.18}$$

Let's consider the linear operator [49, 70],

$$L\left[u\right] = \frac{\partial u}{\partial t}, \tag{5.19}$$

satisfying,

$$L\left[u\right]=0\Leftrightarrow u=u(x). \tag{5.20}$$

Proceed in constructing the R_m term, for $m\geq 1$, having,

$$\begin{cases} R_m(u_{m-1})=\dfrac{1}{(m-1)!}\dfrac{\partial^{m-1}N\left[u\right]}{\partial p^{m-1}}\Big|_{p=0}, \\ \\ N\left[u\right]=\dfrac{\partial u}{\partial t}+\gamma u\dfrac{\partial u}{\partial x}-\alpha\dfrac{\partial^2 u}{\partial x^2}+\beta\dfrac{\partial^3 u}{\partial x^3}, \end{cases} \tag{5.21}$$

which gives,

$$R_m(u_{m-1})=\frac{\partial u_{m-1}}{\partial t}+\gamma\left(\sum_{k=0}^{m-1}\frac{\partial u_k}{\partial x}u_{m-1-k}\right)-\alpha\frac{\partial^2 u_{m-1}}{\partial x^2}+\beta\frac{\partial^3 u_{m-1}}{\partial x^3}. \tag{5.22}$$

Then, the m th order deformation equation is obtained as,

$$\begin{cases} L\left[u_m-\chi_m u_{m-1}\right]=\hbar R_m(u_{m-1}), \\ \\ u_m(x,0)=\begin{cases} u(x,0), & m=1 \\ 0, & \text{otherwise} \end{cases}, \quad \chi_m=\begin{cases} 0, & m=1 \\ 1, & \text{otherwise} \end{cases} \end{cases} \tag{5.23}$$

Using equation (5.19), equation (5.23) can be rewritten as,

$$\begin{cases} \dfrac{\partial u_m}{\partial t}-\chi_m\dfrac{\partial u_{m-1}}{\partial t}=\hbar\left(\dfrac{\partial u_{m-1}}{\partial t}+\gamma\left(\sum_{k=0}^{m-1}\dfrac{\partial u_k}{\partial x}u_{m-1-k}\right)-\alpha\dfrac{\partial^2 u_{m-1}}{\partial x^2}+\beta\dfrac{\partial^3 u_{m-1}}{\partial x^3}\right), \\ \\ u_m(x,0)=\begin{cases} u(x,0), & m=1 \\ 0, & \text{otherwise} \end{cases}, \quad \chi_m=\begin{cases} 0, & m=1 \\ 1, & \text{otherwise} \end{cases} \end{cases} \tag{5.24}$$

The latter system is recursively solved for u_m by utilizing Mathematica where, respecting the $\hbar$-curve analysis, $\hbar=0.01$ is chosen. A 6th order approximation, reveals an error, $||\delta||_\infty=9.3\times 10^{-6}$. The topic of convergence is thoroughly analyzed in [58].

5.3.2 The homotopy method for the viscous Burgers equation

Following the same procedure as in the KdV–B equation, the initial guess,

$$u(x,0)=\frac{\mathrm{e}^{-x}}{1+\mathrm{e}^{-x}}, \tag{5.25}$$

is proposed. A 7th order approximation, reveals an error, $||\delta||_\infty=1.8\times 10^{-5}$.

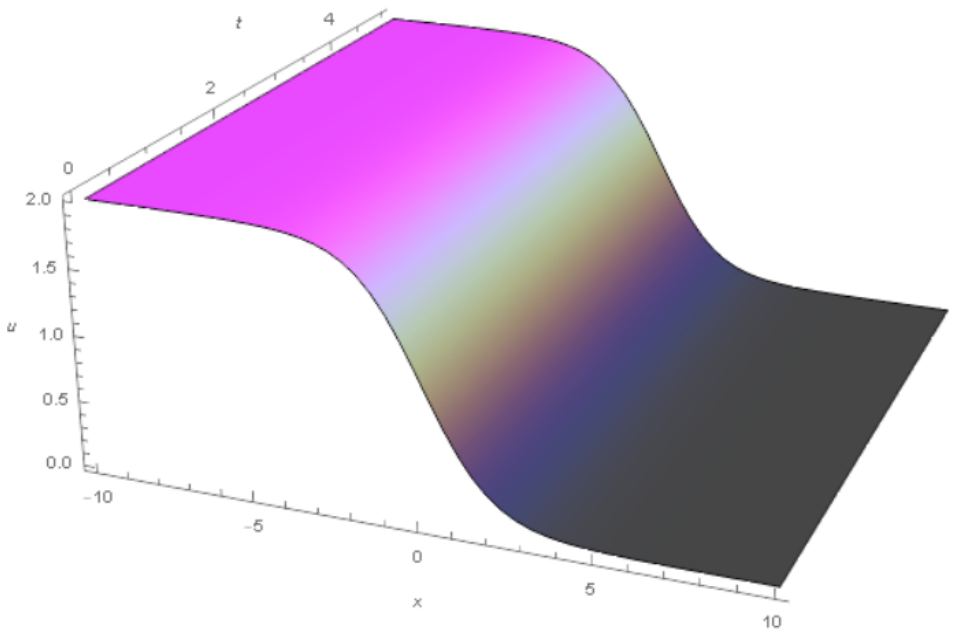

Figure 5.6: A homotopy solution of 6th order to the KdV–B equation, for the values of $\alpha = 0.1$, $\beta = 0.01$ $\gamma = 0.5$ and $\hbar = 0.01$, with $(x, t) \in [-10, 10] \times [0, 5]$.

CHAPTER 6

Pulse Interactions in Fluid Dynamics

6.1 The Boussinesq equation

The normalized Boussinesq equation, reads [52],

$$u_{tt} - u_{xx} - 3\left(u^2\right)_{xx} - u_{xxxx} = 0, \quad u = u(x,t), \quad (x,t) \in \mathbb{R} \times (0,\infty). \quad (6.1)$$

Derived in 1872 by Boussinesq, (6.1) and its modifications can mathematically describe blood flow dynamics. [32, 64].

Application of the traveling wave transform (3.8), seeking for pulse solutions, leads to the bidirectional pulse solution,

$$u(x,t) = \frac{\lambda^2 - 1}{2}\operatorname{sech}^2\left(\frac{\sqrt{\lambda^2-1}}{2}(x - \lambda t - c)\right), \quad c \in \mathbb{R}, \quad |\lambda| \geq 1. \quad (6.2)$$

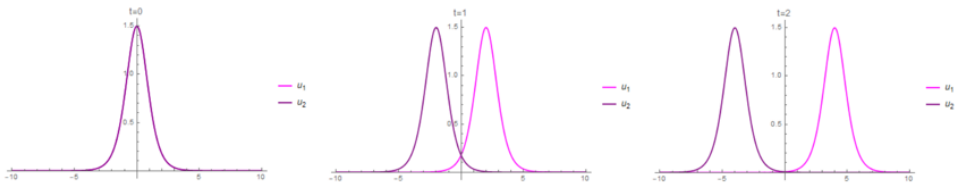

Figure 6.1: A right-, u_1, and left-, u_2, pulse solutions of the Boussinesq equation, for the values of $\lambda_1 = 2$ and $\lambda_2 = -2$, with $(x,t) \in [-10,10] \times \{0,1,2\}$.

6.1.1 The Spectral Scheme for the Boussinesq equation

The spectral scheme in this case is,

$$\begin{cases} c_n = \dfrac{\displaystyle\int_{-\infty}^{\infty} (\kappa^2 + \lambda^2 - 1)|\hat{v_n}|^2 d\kappa}{\displaystyle 3\int_{-\infty}^{\infty} F\left\{v_n^2\right\} \hat{v_n}^* d\kappa}, \\ \hat{v_{n+1}} = \dfrac{3c_n F\{v_n^2\} + (1 - \lambda^2 + R)\hat{v_n}}{\kappa^2 + R}, \quad R > 0 \end{cases} \tag{6.3}$$

Here, $R > 0$ prevents the denominator in $\hat{v_{n+1}}$ from equaling zero and thus the scheme from diverging.

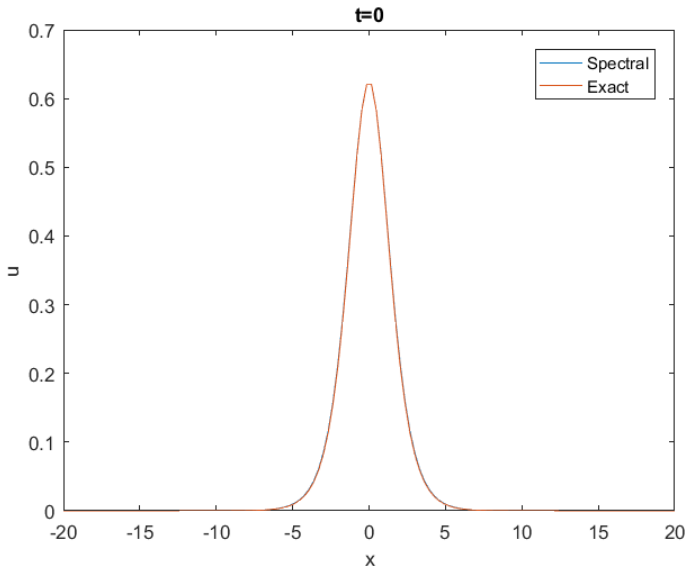

Figure 6.2: The spectral solution and the exact solution of the Boussinesq equation, for the values of $\lambda = 1.5$ and $R = 1$, with $(x, t) \in [-20, 20] \times \{0\}$.

6.2 The Benjamin–Bona–Mahony (BBM) equation

The Benjamin–Bona–Mahony (BBM) equation, reads [19],

$$u_t + u_x + uu_x - u_{txx} = 0, \quad u = u(x, t), \quad (x, t) \in \mathbb{R} \times (0, \infty). \tag{6.4}$$

Studied by Bengamin, Bona and Mahony in 1972, to mathematically model unidirectional propagating waves, simulating, in a sense, the cardiac pulse.

Application of the traveling wave transform (3.8), seeking for pulse solutions, leads to the first order separable ODE,

$$(1-\lambda)u^2(\zeta)+\frac{u^3(\zeta)}{3}+\lambda(u'(\zeta))^2=0 \tag{6.5}$$

with its solution being,

$$u(x,t)=3(\lambda-1)\mathrm{sech}^2\left(\frac{1}{2}\sqrt{\frac{\lambda-1}{\lambda}}\,(x-\lambda t-c)\right),\quad c\in\mathbb{R}. \tag{6.6}$$

6.2.1 The Spectral Scheme for BBM

The spectral scheme in this case is,

$$\begin{cases} \hat{v_{n+1}}=\dfrac{\frac{c_n}{2}F\{v_n^2\}+(1-\lambda+R)\hat{v_n}}{\lambda\kappa^2+R},\quad R>0,\\[2ex] c_n=\dfrac{2\displaystyle\int_{-\infty}^{\infty}(\lambda\kappa^2-1+\lambda)|\hat{v_n}|^2d\kappa}{\displaystyle\int_{-\infty}^{\infty}F\left\{v_n^2\right\}\hat{v_n}^*d\kappa} \end{cases} \tag{6.7}$$

6.2.2 Multi-pulse interactions

Following the same approach as in the KdV case, one obtains a 2-pulse solution of BBM, as [10, 44, 78],

$$u=u(x,t)=\frac{12}{1-\kappa_1^2}\left(\log(f(x,t))_{xx}\right., \tag{6.8}$$

with,

$$f(x,t)=1+\mathrm{e}^{\zeta_1}+\mathrm{e}^{\zeta_2}+B\,\mathrm{e}^{\zeta_1+\zeta_2},\quad \zeta_1=\kappa_1x-\frac{\kappa_1}{1-\kappa_1^2}t-c_1,\quad \zeta_2=\kappa_2x-\frac{\kappa_2}{1-\kappa_2^2}t-c_2, \tag{6.9}$$

with $|\kappa_1|\neq|\kappa_2|$ and $B=\left(\dfrac{\kappa_1-\kappa_2}{\kappa_1+\kappa_2}\right)^2$. Again, $B\neq0$ expresses the phase shift term.

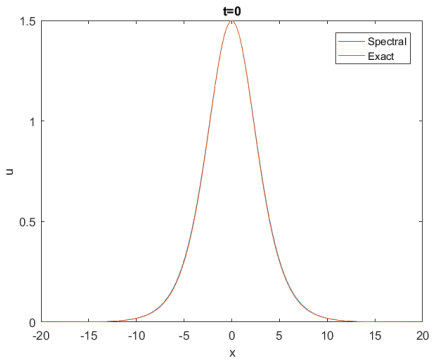

Figure 6.3: The spectral solution and the exact solution of the BBM equation, for the values of $\lambda = 1.5$ and $R = 1$, with $(x, t) \in [-40, 40] \times \{0\}$.

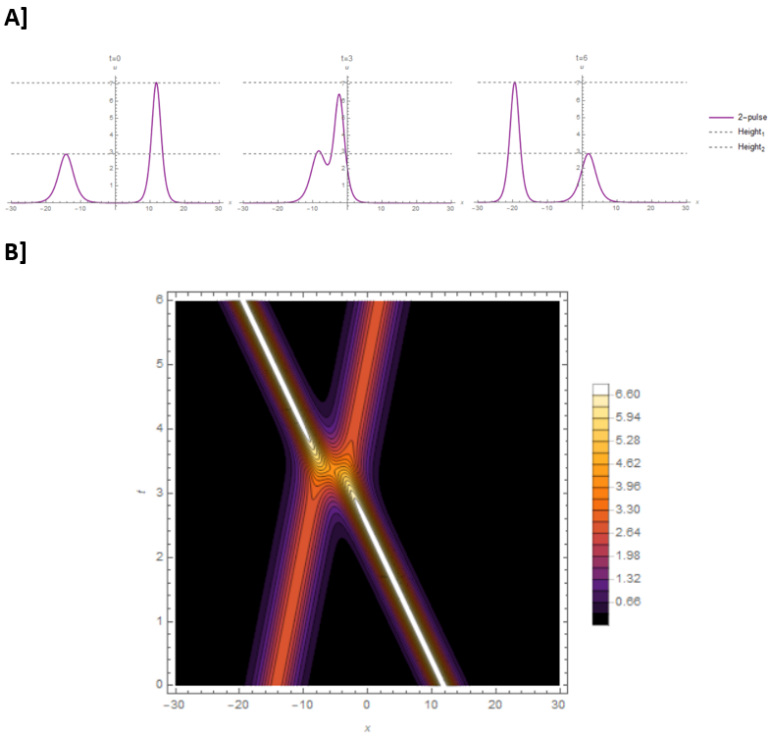

Figure 6.4: [A] Time evolution of a 2-pulse of BBM. [B] A 2-pulse solution of BBM, exhibiting an elastic interaction, for the values of $\kappa_1 = 0.7$, $\kappa_2 = 1.1$, $c_1 = -10$ and $c_2 = 10$ with $(x, t) \in [-30, 30] \times [0, 6]$.

6.3 Camassa–Holm & Degasperis–Procesi equations

In fluid dynamics, the Camassa–Holm (CH) PDE reads [21, 24, 39],

$$u_t - u_{txx} + 3uu_x + 2\alpha u_x = 2u_x u_{xx} + uu_{xxx}, \quad u = u(x,t), \quad (x,t) \in \mathbb{R}\times(0,\infty), \quad \alpha \geq 0. \tag{6.10}$$

Finding, if possible, traveling wave solutions that break, partially motivated the discovery of the CH equation in 1993, from the assymptotic analysis of the Eulerian hydrodynamic equations [21, 39]. The CH mathematical model predicts unidirectional wave propagation.

The Degasperis–Procesi (DP) PDE [25, 29],

$$u_t - u_{txx} + 4uu_x + 2\alpha u_x = 3u_x u_{xx} + uu_{xxx}, \quad u = u(x,t), \quad (x,t) \in \mathbb{R}\times(0,\infty), \quad \alpha \geq 0, \tag{6.11}$$

is one of only two, the other being the CH equation, exactly solvable [28] PDEs in the following family,

$$u_t - u_{txx} + (b+1)uu_x + 2\alpha u_x = bu_x u_{xx} + uu_{xxx}, \quad \alpha \geq 0, \quad b = 2, 3. \tag{6.12}$$

In 1998, the search for similar equations to the CH PDE, led into deriving the DP PDE. The case of $\alpha > 0$ has later been found to exhibit an asymptotic accuracy equal to the CH equation [25, 53].

6.3.1 Phase plane analysis

In search for solutions vanishing at both infinities, the traveling wave transform (3.8) reduces the CH equation to,

$$(2\alpha - \lambda)u(\zeta) + \lambda u''(\zeta) + \frac{3}{2}u^2(\zeta) = \frac{1}{2}(u'(\zeta))^2 + u(\zeta)u''(\zeta) \tag{6.13}$$

and the DP equation to,

$$(2\alpha - \lambda)u(\zeta) + \lambda u''(\zeta) + 2u^2(\zeta) = (u'(\zeta))^2 + u(\zeta)u''(\zeta). \tag{6.14}$$

Notice that, (6.13) reduces to,

$$\begin{cases} u' = v, \\ \\ v' = \dfrac{v^2 - 3u^2 - 2(2\alpha - \lambda)u}{2(\lambda - u)} \end{cases} \tag{6.15}$$

whereas (6.14) to,

$$\begin{cases} u' = v, \\ \\ v' = \dfrac{v^2 - 2u^2 - (2\alpha - \lambda)u}{\lambda - u} \end{cases} \tag{6.16}$$

The critical points are,

$$\begin{cases} P(0,0), \\ \\ Q\left(\dfrac{2\lambda - 4\alpha}{3}, 0\right) \end{cases} \quad \text{and} \quad \begin{cases} P'(0,0), \\ \\ Q'\left(\dfrac{\lambda - 2\alpha}{2}, 0\right) \end{cases} \tag{6.17}$$

for CH and DP, respectively.

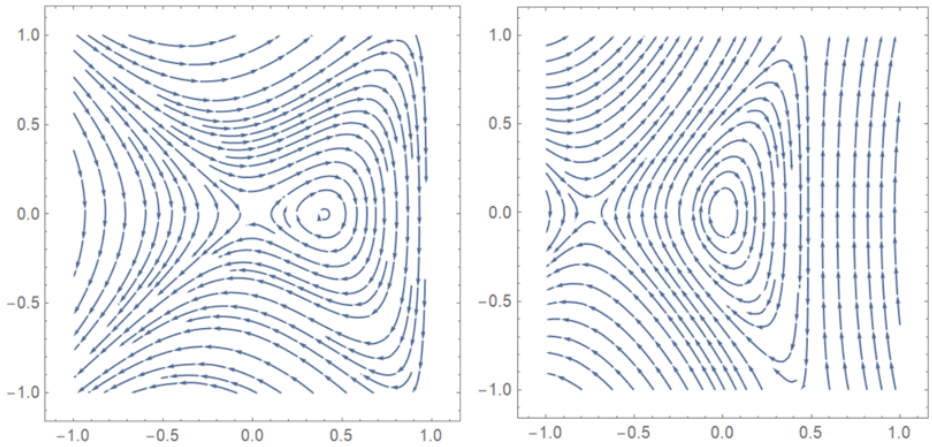

Figure 6.5: The phase plane trajectories for the CH equation (left) and the DP equation (right) for the values of $\{\kappa = 0.2, \lambda = 1\}$ and $\{\kappa = 1, \lambda = 0.5\}$ respectively, both for $(u, v) \in [-1, 1] \times [-1, 1]$.

Remark 17. *1. For $2\alpha > \lambda > 0$, P and P' are central points, implying local stability, whereas Q and Q' are saddle points, implying local non-stability.*

2. For $2\alpha < \lambda$, P and P' are saddle points, whereas Q and Q' are central points.

6.3.2 Weak solution formulation

In the limiting case of $\alpha = 0$ the solitons of equations (6.10) and (6.11) become peaked. The piecewise–differentiability asks for a weak solution interpretation [21].

In terms of the auxiliary function $m(x,t)$, defined as,

$$m := u - u_{xx}, \tag{6.18}$$

equations (6.10) and (6.11) take the simpler form,

$$m_t + m_x u + bmu_x = 0, \tag{6.19}$$

for $b = 2, 3$, with the solution [43],

$$u(x,t) = \lambda \mathrm{e}^{-|x-\lambda t|}, \quad \lambda > 0. \tag{6.20}$$

The latter is a peaked soliton with its height equalling its propagating speed.

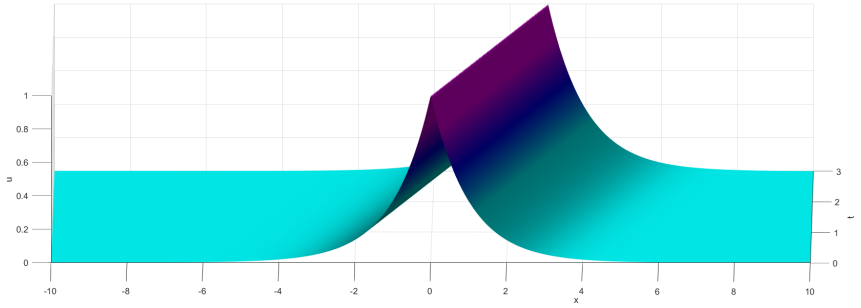

Figure 6.6: A right-moving peaked soliton of (6.19) for the value of $\lambda = 1$ with $(x,t) \in [-10, 10] \times [0, 3]$.

The first derivative's discontinuity at the peak, implies that its u_{xx} is considered in a distributional, weak sense. Let,

$$m = u - u_{xx} = \lambda \delta(x - \lambda t). \tag{6.21}$$

For the product mu_x occurring in the PDE to be defined, take $u_x(0)$ to equal the average of its left and right limits, zero in this case. Alternatively, invert the relationship between u and m by,

$$m = \mathrm{e}^{-|x|} \star u \tag{6.22}$$

and use this to rewrite the PDE in a nonlocal hyperbolic conservative form,

$$u_t + \left[\frac{u^2}{2} + \frac{\mathrm{e}^{-|x|}}{2}\left(\frac{bu^2}{2} + \frac{(3-b)u_x^2}{2}\right)\right]_x = 0. \tag{6.23}$$

In the above setting, u can be understood as a weak solution [26]. Here, $\star$, denotes convolution with respect to x.

6.3.3 Weak Solution Interactions

To obtain a multi–peaked solution, take a linear combination of peaked solitons. The n–peaked solution thus takes the form [15, 33],

$$u(x,t) = \frac{1}{2}\sum_{i=1}^{n} m_i(t)\mathrm{e}^{-2|x-x_i(t)|}, \tag{6.24}$$

representing n interacting travelling waves. Substitution into (6.19) produces a system of ODEs, where in the integrable cases, $b = 2$ and $b = 3$, it is explicitly solvable for arbitrary n by means of inverse spectral techniques.

The two–peaked solution for the CH case is given by [15],

$$\begin{cases} m_1 = -\dfrac{2(\lambda_1^2\alpha_1 + \lambda_2^2\alpha_2)}{\lambda_1\lambda_2(\lambda_1\alpha_1 + \lambda_2\alpha_2)}, \\ x_1 = \dfrac{1}{2}\log\left(\dfrac{2(\lambda_1-\lambda_2)^2\alpha_1\alpha_2}{\lambda_1^2\alpha_1 + \lambda_2^2\alpha_2}\right), \\ m_2 = -\dfrac{2(\alpha_1+\alpha_2)}{\lambda_1\alpha_1 + \lambda_2\alpha_2}, \\ x_2 = \dfrac{1}{2}\log\left(2(\alpha_1+\alpha_2)\right), \end{cases} \tag{6.25}$$

with,

$$\alpha_i(t) = \alpha_i(0)\mathrm{e}^{\frac{t}{\lambda_i}} \tag{6.26}$$

where $\alpha_i(0)$ and λ_i are specified by initial conditions.

Remark 18. *Consideration of symmetric functions of α_i and λ_i, allows to obtain the general solution for arbitrary n. The construction process for the general multi–peaked solution to the DP equation, for $b = 3$, is similar, yet the detailed structure is more complicated [62].*

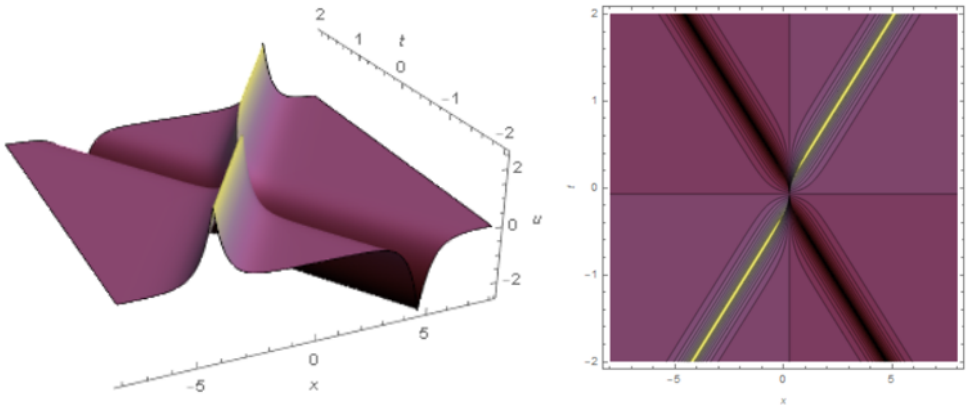

Figure 6.7: A multi-peaked solution of (6.19), exhibiting an elastic interaction, for the values of $\alpha_1(0) = 0.3$, $\alpha_2(0) = 0.6$, $\lambda_1 = 0.4$ and $\lambda_2 = -0.4$, with $(x,t) \in [-8,8] \times [-2,2]$. Again, same as in BBM, notice the recurrent phase shift.

6.3.4 Spectral Schemes for CH and DP

The spectral scheme in the CH case is,

$$\begin{cases} c_n = \dfrac{2\displaystyle\int_{-\infty}^{\infty} (\lambda\kappa^2 - 2\alpha + \lambda)|\hat{v_n}|^2 d\kappa}{\displaystyle\int_{-\infty}^{\infty} F\left\{3v_n^2 - (v_n')^2 - 2v_n v_n''\right\} \hat{v_n}^* d\kappa}, \\ \hat{v_{n+1}} = \dfrac{\frac{1}{2}c_n F\left\{3v_n^2 - (v_n')^2 - 2v_n v_n''\right\} + (2\alpha - \lambda + R)\hat{v_n}}{\lambda\kappa^2 + R}, \quad R > 0 \end{cases} \tag{6.27}$$

The spectral scheme in the DP case is,

$$\begin{cases} c_n = \dfrac{\displaystyle\int_{-\infty}^{\infty} (\lambda\kappa^2 - 2\alpha + \lambda)|\hat{v_n}|^2 d\kappa}{\displaystyle\int_{-\infty}^{\infty} F\left\{2v_n^2 - (v_n')^2 - v_n v_n''\right\} \hat{v_n}^* d\kappa}, \\ \hat{v_{n+1}} = \dfrac{c_n F\left\{2v_n^2 - (v_n')^2 - v_n v_n''\right\} + (2\alpha - \lambda + R)\hat{v_n}}{\lambda\kappa^2 + R}, \quad R > 0 \end{cases} \tag{6.28}$$

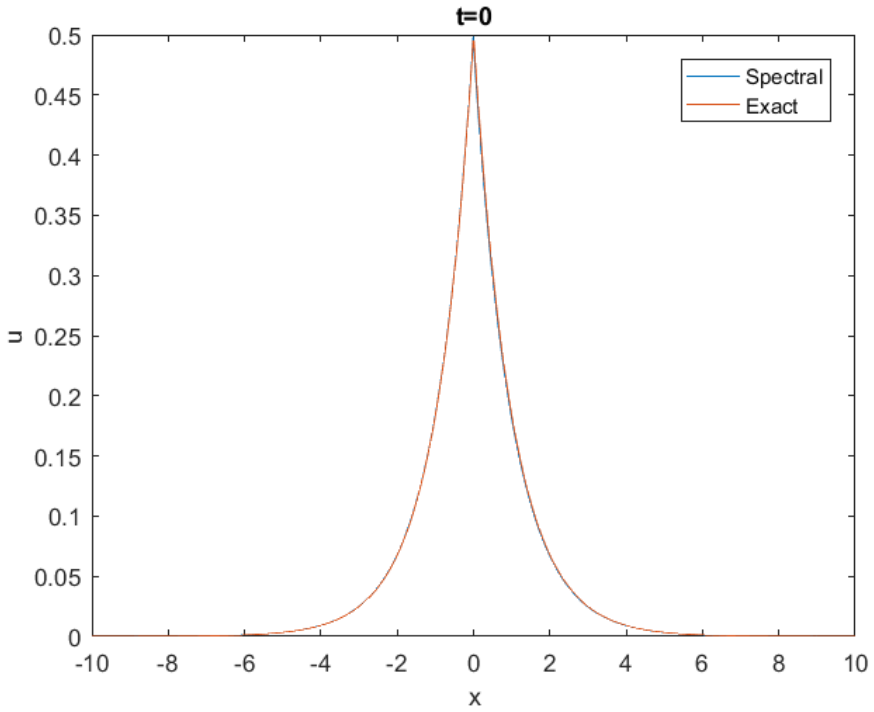

Figure 6.8: The spectral peaked solution and the exact peaked solution of the CH equation, for the values of $\lambda = \frac{1}{2}$, $\alpha = 0$ and $R = 1$, with $(x,t) \in [-10,10] \times \{0\}$.

6.4 The Davey–Stewartson (DS) equation

The Davey–Stewartson (DS) equation [50, 68],

$$\begin{cases} iu_t + \frac{1}{2}\sigma^2 \left(u_{xx} + \sigma^2 u_{yy}\right) + \lambda |u|^2 u - u v_x = 0, \\ \\ v_{xx} - \sigma^2 v_{yy} - 2\lambda \left(|u|^2\right)_x = 0 \end{cases} \tag{6.29}$$

is expressed by a coupled system of PDEs. Here u stands for a complex wave-amplitude field, whereas v denotes a real mean-flow field. Derived by Davey and Stewartson in 1974, the DS PDE is an integrable mathematical model in fluid dynamics [17]. Being a product of multiple-scale analysis, the equation mathematically can model evolving 3-D wave-packets on finite water depth,

ultrasounds and blood flow dynamics [16, 17, 55].

The cases of $\sigma = 1$ and $\sigma = i$ are known as the DS-I and DS-II equations, respectively. The values of λ determine the focusing and defocusing cases. Traveling wave solutions of both the DS-I and DS-II cases will be examined.

Regarding the DS-I case, for $\sigma = 1$, consider,

$$\begin{cases} u(x,y,t) = w(\zeta)\mathrm{e}^{i(\alpha x + y + \mu t)}, \\ v(x,y,t) = v(\zeta), \\ \zeta = x - 2\alpha y + \alpha t, \quad \mu > 0 \end{cases} \tag{6.30}$$

Application of (6.30), transforms (6.29) into,

$$\begin{cases} \frac{1}{2}\left(1+4\alpha^2\right)w'' - \frac{1}{2}\left(\alpha^2+2\mu+1\right)w + \lambda w^3 - wv' = 0, \\ \\ (1-4\alpha^2)v'' - 2\lambda\left(w^2\right)' = 0 \end{cases} \tag{6.31}$$

Let any integration constant equal zero. Integrating the second equation of (6.31), provides with,

$$\begin{cases} \frac{1}{2}\left(1+4\alpha^2\right)w'' - \frac{1}{2}\left(\alpha^2+2\mu+1\right)w + \lambda w^3 - wv' = 0, \\ \\ v' = \dfrac{2\lambda}{1-4\alpha^2}w^2 \end{cases} \tag{6.32}$$

Therefore, one is now led to the second order ODE for $w(\zeta)$,

$$w'' - \frac{\alpha^2+2\mu+1}{4\alpha^2+1}w - \frac{2\lambda}{1-4\alpha^2}w^3 = 0. \tag{6.33}$$

Multiplying by w' and integrating, results to the separable first order equation,

$$\left(w'\right)^2 = q_1 w^2 - q_2 w^4 \tag{6.34}$$

with,

$$\begin{cases} q_1 = \dfrac{\alpha^2+2\mu+1}{4\alpha^2+1}, \\ \\ q_2 = \dfrac{\lambda}{4\alpha^2-1} \end{cases} \tag{6.35}$$

Now, (6.34) admits the solution,

$$w(\zeta) = \sqrt{\frac{q_1}{q_2}}\operatorname{sech}\left(\sqrt{q_1}\zeta\right) \tag{6.36}$$

for,

$$\lambda\left(4\alpha^2 - 1\right) > 0. \tag{6.37}$$

Therefore, one obtains,

$$\begin{cases} w(\zeta) = \sqrt{\dfrac{q_1}{q_2}}\operatorname{sech}\left(\sqrt{q_1}\zeta\right), \\ \\ v = \displaystyle\int \frac{2\lambda}{1-4\alpha^2} w^2 \, d\zeta \end{cases} \tag{6.38}$$

or equivalenty,

$$\begin{cases} w(\zeta) = \sqrt{\dfrac{q_1}{q_2}}\operatorname{sech}\left(\sqrt{q_1}\zeta\right), \\ \\ v = -2\sqrt{q_1}\tanh\left(\sqrt{q_1}\zeta\right) \end{cases} \tag{6.39}$$

Finally, using (6.30), (6.39) ultimately reads,

$$\begin{cases} u(x,y,t) = \sqrt{\dfrac{(4\alpha^2-1)(\alpha^2+2\mu+1)}{\lambda(4\alpha^2+1)}}\operatorname{sech}\left(\sqrt{\dfrac{\alpha^2+2\mu+1}{4\alpha^2+1}}\left(x-2\alpha y+\alpha t\right)\right)\mathrm{e}^{i(\alpha x+y+\mu t)}, \\ \\ v(x,y,t) = -2\sqrt{\dfrac{\alpha^2+2\mu+1}{4\alpha^2+1}}\tanh\left(\sqrt{\dfrac{\alpha^2+2\mu+1}{4\alpha^2+1}}\left(x-2\alpha y+\alpha t\right)\right) \end{cases} \tag{6.40}$$

Regarding the DS-II case, for $\sigma = i$, consider,

$$\begin{cases} u(x,y,t) = w(\xi)\mathrm{e}^{i(\alpha x+y+\mu t)}, \\ v(x,y,t) = v(\xi), \\ \xi = x + 2\alpha y - \alpha t, \quad \mu > 0 \end{cases} \tag{6.41}$$

and follow the same steps as for the DS-I case.

Ultimately, one obtains,

$$\begin{cases} u(x,y,t) = \sqrt{\dfrac{(1+4\alpha^2)(\alpha^2-2\mu-1)}{\lambda(1-4\alpha^2)}}\operatorname{sech}\left(\sqrt{\dfrac{\alpha^2-2\mu-1}{1-4\alpha^2}}\,(x+2\alpha y-\alpha t)\right)\mathrm{e}^{i(\alpha x+y+\mu t)}, \\ v(x,y,t) = -2\sqrt{\dfrac{\alpha^2-2\mu-1}{1-4\alpha^2}}\tanh\left(\sqrt{\dfrac{\alpha^2-2\mu-1}{1-4\alpha^2}}\,(x+2\alpha y-\alpha t)\right) \end{cases} \tag{6.42}$$

Remark 19. *The solution pairs of* (6.40) *and* (6.42) *are denoted as the 1-soliton solutions of DS-I and DS-II, respectively.*

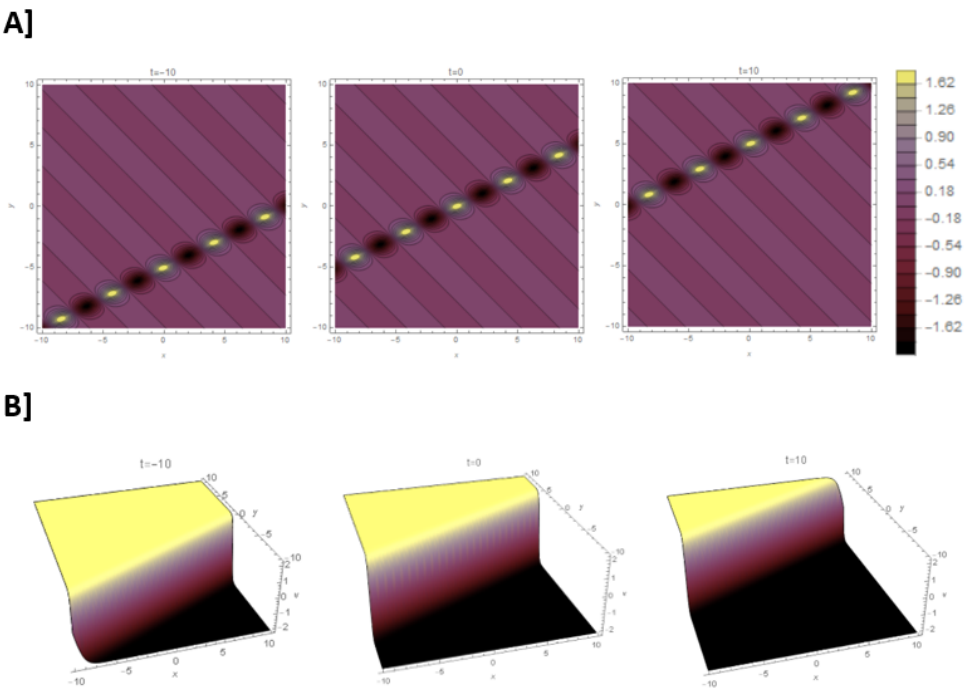

Figure 6.9: [A] The real part of a breather solution, u, of the DS-I system, for the values of $\lambda = \alpha = 1$ and $\mu = 2$, with $(x,t) \in [-10,10] \times \{-10,0,10\}$. [B] The corresponding wavefront velocity v. Notice that the two propagate at the same direction.

6.5 Future Steps

The future research plans are summarized in examining Fluid-Structure Interactions (FSI) in cardiac hemodynamics, as well as time-evolving real-life cardiovascular data by means of KdV–B.

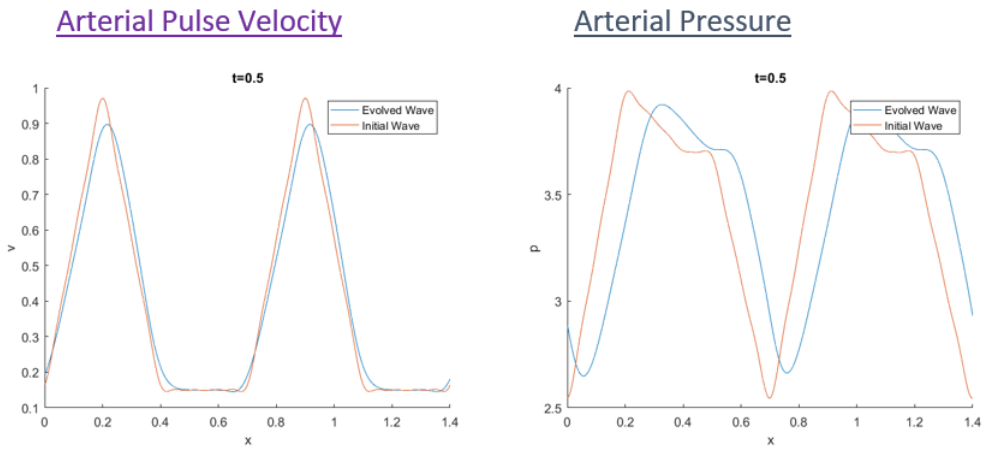

Figure 6.10: Arterial pulse and pressure waveforms, time-evolved by KdV–B.

Remark 20. *As of current analysis, the KdV–B mathematical model seems to be quite reliable as a cardiac hemodynamics model.*

CHAPTER 7

Conclusions

Nonlinearity arises in a plethora of fluid dynamics applications, ranging from hydrodynamics to cardiac and neuronal dynamics. Nonlinear dynamical systems may exhibit an unpredictable and counter-intuitive behaviour contrasting with simplified linear systems. There's no unified theory tackling nonlinearity, implying that different techniques are used for different problems of fluid dynamics.

Complex phenomena in fluid dynamics, cardiac and neuronal dynamics, can be mathematically modeled in terms of Korteweg–de Vries–Burgers (KdV–B)-, Boussinesq-, Burgers–Huxley (BH)-type and Womersley equations.

A mixture of analytic, semi-analytic and approximate methods was implemented for the behavior of solutions to these equations. Semi-exact solutions were derived by a homotopy analysis approach. Numerical solutions were derived by means of spectral Fourier analysis and were evolved in time, using the 4th order explicit Runge–Kutta method.

The remarkable solitonic properties were also studied through a computational spectral Fourier approach. A modification to the method was discussed for wavefront solutions. The spectral approach, being a method of spectral accuracy, regarding the spatial variables, continuously balances the ratio of dispersion and nonlinearity of the PDE, converging rapidly to a solution of the required accuracy.

Additionally, weak solution formulation was discussed for the CH, DP and inviscid Burgers PDEs. In the latter, qualitative analysis was also performed on more general scalar hyperbolic conservative forms. Phase plane trajectories were obtained for the KdV–B, CH and DP equations.

Notable exact results regarding pulse interactions, line solitons, multi-shock fusion, peaked solitary waves, and pulsatile waveforms were obtained. Exact,

semi-exact and numerical solutions were compared and discussed in detail.

The derivation of analytical solutions to the aforementioned mathematical models, is a process of high significance. Such solutions are used to benchmark numerical solvers, perform stability analysis and grasp a better understanding of the studied models. This whole analysis provided vital information on the connection and applicability of these fundamental equations to fluid dynamics and its related fields of active research.

Appendix

The dispersion relation

A linear wave, $u(x,t)$ can be represented by Fourier components, in plane wave form,

$$u(x,t) = \Re\{A\mathrm{e}^{i(\kappa x - \omega t)}\} \tag{1}$$

with κ denoting the wavenumber, ω the frequency and A the wave amplitude. Additionally, $\Re\{\cdot\}$ denotes the real part function. Both ω and A may solely depend on κ. The dispersion relation,

$$\omega = \omega(\kappa) \tag{2}$$

governs linear wave dynamics. Different linear mathematical models are characterized by different dispersion relations. As an example consider the linearized BBM equation,

$$u_t + u_x - u_{xxt} = 0. \tag{3}$$

Substituting $\mathrm{e}^{i(\kappa x - \omega t)}$ into (3), provides with the dispersion relation,

$$\omega(\kappa) = \frac{\kappa}{1-\kappa^2}, \quad \kappa \neq \pm 1. \tag{4}$$

Generally, these relations describe the way dispersion affects wave propagation in a medium. Obtaining the dispersion relation, allows calculating both the phase and group velocities as functions of ω.

Phase and group velocity

The phase velocity, also known as celerity, of a wave denotes its rate of propagation. Any of the frequency components travels at phase velocity. For instance, the wave crest travels with the phase velocity. For a nonzero wavenumber, the phase velocity is defined as,

$$v_p := \frac{\omega(\kappa)}{\kappa}. \tag{5}$$

A sea state can be viewed as a superposition of sinusoidal waves of different wavelengths, amplitudes, initial phases and propagation directions. Each component travels with its own phase velocity.

Regarding the group velocity of a wave, it denotes the speed at which the energy of the wave propagates [97]. Equivalently, it refers to the energy transport velocity. It's defined as,

$$v_g := \omega'(\kappa). \tag{6}$$

For water waves, the energy is given by [97],

$$E := g\frac{|A|^2}{2} \tag{7}$$

with g being the gravitational acceleration. In shallow waters, the two aforementioned velocities are equal, since shallow water waves lack dispersion. On the contrary, for deep waters, the group velocity is half the phase velocity [97].

The Painleve property

An ODE exhibits the Painleve property, whenever it admits no movable singularities. A movable singularity is a point where the solution either becomes undefined or lacks regularity, whose location is dependant on the arbitrary constants of integration [96].

For instance, the equation,

$$y'(x) = y^2(x), \tag{8}$$

has the solution,

$$y(x) = (C - x)^{-1} \tag{9}$$

exhibiting a movable singularity whenever x equals C. Therefore, it fails to possess the Painleve property.

The Inverse Scattering Transform (IST)

The IST serves as a nonlinear and more general analogue of the Fourier Transform, with the latter applied to linear PDEs. The transform's key idea is recovering a potential's time evolution from the one of its scattering data. Inverse scattering recovers a potential from its scattering matrix, opposed to direct scattering obtaning the scattering matrix from the potential. More precisely, the solution of the Cauchy problem is expressed in terms of the solution of a linear equation. Since the latter is formulated in terms of spectral functions, defined by the initial data, the solution formula is effective [4, 66].

On the nature of rarefaction waves

In physical applications, a rarefaction wave succeeds a shock wave, being an area of low relative pressure. Rarefaction propagates oppositely to the acceleration of the fluid particles, in contrary to a shock, where acceleration occurs along the shock [67]. A natural rarefaction happens in the Earth's atmosphere. Mass leads to most atmospheric matter being near to Earth due to gravitation. Thus, in comparison to the lowest atmospheric layers, air at higher layers is less dense, or rarefied. Rarefaction is easily observed when a spring is compressed and released [48].

The Fourier and Inverse Fourier Transforms

The Fourier Transform, and its inverse, of function u, are defined as [5, 61],

$$\begin{cases} F\left\{u(x)\right\} = \hat{u}(k) = \displaystyle\int_{-\infty}^{\infty} \mathrm{e}^{-ikx} u(x)dx, \\ \\ F^{-1}\left\{\hat{u}(k)\right\} = u(x) = \dfrac{1}{2\pi}\displaystyle\int_{-\infty}^{\infty} \mathrm{e}^{ikx}\hat{u}(k)dk \end{cases} \tag{10}$$

Integrating by parts, regarding the nth derivative of f and its Fourier Transform, the following results hold,

$$\begin{cases} \dfrac{d^n u}{dx^n} = (i^n)F^{-1}\left\{k^n \hat{u}(k)\right\}, \\ \\ \dfrac{d^n \hat{u}}{dx^n} = (-i)^n F\left\{x^n u(x)\right\} \end{cases} \tag{11}$$

Generalizing to n dimensions, the respected n-D Fourier and Inverse Fourier Transform, are defined as,

$$\begin{cases} F\left\{u(\vec{x})\right\} = \hat{u}(\vec{\kappa}) = \displaystyle\int_{-\infty}^{\infty} \mathrm{e}^{-i\vec{\kappa}\cdot\vec{x}} u(\vec{x}) d\vec{x}, \\ \\ F^{-1}\left\{\hat{u}(\vec{\kappa})\right\} = u(\vec{x}) = \dfrac{1}{2\pi} \displaystyle\int_{-\infty}^{\infty} \mathrm{e}^{i\vec{\kappa}\cdot\vec{x}} \hat{u}(\vec{\kappa}) d\vec{\kappa} \end{cases} \tag{12}$$

Being an integral transform, the Fourier Transform preserves both linearity and homogeneity.

The notion of homotopy

Definition 13. *A homotopy between two continuous functions f and g from a topological space X to a topological space Y is a continuous function $H : X \times [0,1] \to Y$, satisfying,*

$$\begin{cases} H(x,0) = f(x), \\ H(x,1) = g(x), \quad \textit{for all} \quad x \in X \ [12]. \end{cases} \tag{13}$$

Practically, the two functions can continuously deform into each other.

Bibliography

[1] Ablowitz, M., Fokas, A., and Musslimani, Z. On a new non-local formulation of water waves. *Journal of Fluid Mechanics 562* (2006), 313–343.

[2] Ablowitz, M., and Horikis, T. Solitons and spectral renormalization methods in nonlinear optics. *The European Physical Journal Special Topics 173*, 1 (2009), 147–166.

[3] Ablowitz, M. J. *Nonlinear dispersive waves: asymptotic analysis and solitons*, vol. 47. Cambridge University Press, 2011.

[4] Ablowitz, M. J., and Clarkson, P. A. *Solitons, nonlinear evolution equations and inverse scattering*, vol. 149. Cambridge university press, 1991.

[5] Ablowitz, M. J., Kaup, D. J., Newell, A. C., and Segur, H. The inverse scattering transform-fourier analysis for nonlinear problems. *Studies in Applied Mathematics 53*, 4 (1974), 249–315.

[6] Ablowitz, M. J., and Musslimani, Z. H. Spectral renormalization method for computing self–localized solutions to nonlinear systems. *Optics letters 30*, 16 (2005), 2140–2142.

[7] Ablowitz, M. J., and Segur, H. *Solitons and the inverse scattering transform*. SIAM, 1981.

[8] Abramowitz, M., Stegun, I. A., and Romer, R. H. Handbook of mathematical functions with formulas, graphs, and mathematical tables, 1988.

[9] Adomian, G. Solving frontier problems of physics: the decomposition method, with a preface by yves cherruault. *Fundamental Theories of Physics, Kluwer Academic Publishers Group, Dordrecht 1* (1994).

[10] Alsayyed, O., Jaradat, H., Jaradat, M., Mustafa, Z., and Shatat, F. Multi-soliton solutions of the bbm equation arisen in shallow water. *J. Nonlinear Sci. Appl 9*, 4 (2016), 1807–1814.

[11] Antar, N., and Demiray, H. Weakly nonlinear waves in a prestressed thin elastic tube containing a viscous fluid. *International journal of engineering science 37*, 14 (1999), 1859–1876.

[12] Armstrong, M. A. *Basic topology*. Springer Science & Business Media, 2013.

[13] Baldwin, D., Göktaş, Ü., Hereman, W., Hong, L., Martino, R., and Miller, J. Symbolic computation of exact solutions expressible in hyperbolic and elliptic functions for nonlinear pdes. *Journal of Symbolic Computation 37*, 6 (2004), 669–705.

[14] Batchelor, C. K., and Batchelor, G. *An introduction to fluid dynamics*. Cambridge university press, 2000.

[15] Beals, R., Sattinger, D. H., and Szmigielski, J. Multipeakons and the classical moment problem. *Advances in Mathematics 154*, 2 (2000), 229–257.

[16] Bi, Y., Zhang, Z., Liu, Q., and Liu, T. Research on nonlinear waves of blood flow in arterial vessels. *Communications in Nonlinear Science and Numerical Simulation* (2021), 105918.

[17] Boiti, M., Martina, L., and Pempinelli, F. Multidimensional localized solitons. *Chaos, Solitons & Fractals 5*, 12 (1995), 2377–2417.

[18] Bona, J., and Schonbek, M. Travelling–wave solutions to the korteweg–de vries–burgers equation. *Proceedings of the Royal Society of Edinburgh Sect A 101* (1985), 207–226.

[19] Bona, J. L., Pritchard, W., and Scott, L. R. Solitary-wave interaction. *The Physics of Fluids 23*, 3 (1980), 438–441.

[20] Bullough, R. K., and Caudrey, P. J. *Solitons*, vol. 17. Springer Science & Business Media, 2013.

[21] Camassa, R., and Holm, D. D. An integrable shallow water equation with peaked solitons. *Physical review letters 71*, 11 (1993), 1661.

[22] Cao, C., Holm, D. D., and Titi, E. S. Traveling wave solutions for a class of one-dimensional nonlinear shallow water wave models. *Journal of Dynamics and Differential Equations 16*, 1 (2004), 167–178.

[23] Chen, Y., and Liu, J. Uniformly valid solution of limit cycle of the duffing–van der pol equation. *Mechanics Research Communications 36*, 7 (2009), 845–850.

[24] Constantin, A. On the scattering problem for the camassa-holm equation. *Proceedings of the Royal Society of London. Series A: Mathematical, Physical and Engineering Sciences 457*, 2008 (2001), 953–970.

[25] Constantin, A., and Lannes, D. The hydrodynamical relevance of the camassa–holm and degasperis–procesi equations. *Archive for Rational Mechanics and Analysis 192*, 1 (2009), 165–186.

[26] Constantin, A., and McKean, H. P. A shallow water equation on the circle. *Communications on Pure and Applied Mathematics: A Journal Issued by the Courant Institute of Mathematical Sciences 52*, 8 (1999), 949–982.

[27] Cornejo-Pérez, O., and Rosu, H. C. Nonlinear second order ode's: factorizations and particular solutions. *Progress of theoretical physics 114*, 3 (2005), 533–538.

[28] Degasperis, A. Asymptotic integrability. *Symmetry and perturbation theory* (1999), 23–37.

[29] Degasperis, A., Holm, D. D., and Hone, A. N. A new integrable equation with peakon solutions. *Theoretical and Mathematical Physics 133*, 2 (2002), 1463–1474.

[30] Demiray, H. Wave propagation through a viscous fluid contained in a prestressed thin elastic tube. *International journal of engineering science 30*, 11 (1992), 1607–1620.

[31] Demiray, H. A note on the exact travelling wave solution to the kdv–burgers equation. *Wave motion 38*, 4 (2003), 367–369.

[32] Dingemans, M. W. *Water wave propagation over uneven bottoms: Linear wave propagation*, vol. 13. World Scientific, 1997.

[33] Efstathiou, A. G., and Petropoulou, E. N. Peakons of novikov equation via the homotopy analysis method. *Symmetry 13*, 5 (2021), 738.

[34] El, G. A., Hoefer, M. A., and Shearer, M. Expansion shock waves in regularized shallow–water theory. *Proceedings of the Royal Society A: Mathematical, Physical and Engineering Sciences 472*, 2189 (2016), 20160141.

[35] Erbay, H., Erbay, S., and Dost, S. Wave propagation in fluid filled nonlinear viscoelastic tubes. *Acta mechanica 95*, 1-4 (1992), 87–102.

[36] Evans, L. C. Partial differential equations. *Graduate studies in mathematics 19*, 2 (1998).

[37] Feng, Z., and Meng, Q. Exact solution for a two-dimensional kdv-burgers-type equation with nonlinear terms of any order. *Discrete & Continuous Dynamical Systems-B 7*, 2 (2007), 285.

[38] Fokas, A., Himonas, A., and Mantzavinos, D. The nonlinear schrödinger equation on the half-line. *Transactions of the American Mathematical Society 369*, 1 (2017), 681–709.

[39] Fuchssteiner, B., and Fokas, A. S. Symplectic structures, their bäcklund transformations and hereditary symmetries. *Physica D: Nonlinear Phenomena 4*, 1 (1981), 47–66.

[40] Gao, G. A theory of interaction between dissipation and dispersion of turbulence. *SSSMP 28* (1985), 616–627.

[41] Gao, Y.-T., and Tian, B. Generalized tanh method with symbolic computation and generalized shallow water wave equation. *Computers & Mathematics with Applications 33*, 4 (1997), 115–118.

[42] Gelfand, I. M., Silverman, R. A., et al. *Calculus of variations*. Courier Corporation, 2000.

[43] Grayshan, K., and Himonas, A. Equations with peakon traveling wave solutions. *Adv. Dyn. Syst. Appl 8*, 2 (2013), 217–232.

[44] Hirota, R. Exact solution of the kortewe–de vries equation for multiple collisions of solitons. *Physical Review Letters 27*, 18 (1971), 1192.

[45] Hirota, R. Direct method of finding exact solutions of nonlinear evolution equations. In *Bäcklund transformations, the inverse scattering method, solitons, and their applications*. Springer, 1976, pp. 40–68.

[46] Horikis, T. P., and Frantzeskakis, D. J. Asymptotic reductions and solitons of nonlocal nonlinear schrödinger equations. *Journal of Physics A: Mathematical and Theoretical 49*, 20 (2016), 205202.

[47] Horikis, T. P., and Frantzeskakis, D. J. Light meets water in nonlocal media: surface tension analogue in optics. *Physical review letters 118*, 24 (2017), 243903.

[48] Ivashnev, O., Ivashneva, M., and Smirnov, N. Rarefaction waves in nonequilibrium-boiling fluid flows. *Fluid Dynamics 35*, 4 (2000), 485–495.

[49] Jafari, H., and Firoozjaee, M. Homotopy analysis method for solving kdv equations. *Surveys in Mathematics and its Applications 5* (2010), 89–98.

[50] Jafari, H., Sooraki, A., Talebi, Y., and Biswas, A. The first integral method and traveling wave solutions to davey–stewartson equation. *Nonlinear Analysis: Modelling and Control 17*, 2 (2012), 182–193.

[51] Jiang, H.-J., Xiang, J.-J., Dai, C.-Q., and Wang, Y.-Y. Nonautonomous bright soliton solutions on continuous wave and cnoidal wave backgrounds in blood vessels. *Nonlinear Dynamics 75*, 1 (2014), 201–207.

[52] Johnson, R. S. *A modern introduction to the mathematical theory of water waves*. No. 19. Cambridge university press, 1997.

[53] Johnson, R. S. The classical problem of water waves: a reservoir of integrable and nearly-integrable equations. *Journal of Nonlinear Mathematical Physics 10*, sup1 (2003), 72–92.

[54] Kadomtsev, B. B., and Petviashvili, V. I. On the stability of solitary waves in weakly dispersing media. In *Sov. Phys. Dokl* (1970), vol. 15, pp. 539–541.

[55] Khismatullin, D., and Akhatov, I. S. Sound–ultrasound interaction in bubbly fluids: Theory and possible applications. *Physics of Fluids 13*, 12 (2001), 3582–3598.

[56] Liang, S., and Jeffrey, D. J. Comparison of homotopy analysis method and homotopy perturbation method through an evolution equation. *Communications in Nonlinear Science and Numerical Simulation 14*, 12 (2009), 4057–4064.

[57] Liao, S. An explicit, totally analytical approximate solution for blasius equation [j]. *Int. J. Non-Linear Mech 34* (1999), 759–778.

[58] Liao, S. *Beyond perturbation: introduction to the homotopy analysis method*. CRC press, 2003.

[59] Liao, S. *Homotopy analysis method in nonlinear differential equations*. Springer, 2012.

[60] Liao, S. Do peaked solitary water waves indeed exist? *Communications in Nonlinear Science and Numerical Simulation 19*, 6 (2014), 1792–1821.

[61] Logan, J. D. *Applied mathematics*. John Wiley & Sons, 2013.

[62] Lundmark, H., and Szmigielski, J. Degasperis-procesi peakons and the discrete cubic string. *International Mathematics Research Papers 2005*, 2 (2005), 53–116.

[63] Ma, W.-X. Lump solutions to the kadomtsev–petviashvili equation. *Physics Letters A 379*, 36 (2015), 1975–1978.

[64] Malatos, M., Raptis, A., Xenos, M. A., Kouvelos, G., Giannoukas, A., and Verhoeven, E. A multiscale model for hemodynamic properties prediction after fenestrated endovascular aneurysm repair. a pilot study. *Hell. Vasc. J 1*, 2 (2019), 73–79.

[65] Malfliet, W., and Hereman, W. The tanh method: I exact solutions of nonlinear evolution and wave equations. *Phys. Scripta 54* (1996), 563–568.

[66] Marchenko, V. A. *Sturm-Liouville operators and applications*, vol. 373. American Mathematical Soc., 2011.

[67] Matsumura, A., and Nishihara, K. Global stability of the rarefaction wave of a one-dimensional model system for compressible viscous gas. *Communications in mathematical physics 144*, 2 (1992), 325–335.

[68] McConnell, M., Fokas, A. S., and Pelloni, B. Localised coherent solutions of the dsi and dsii equations–a numerical study. *Mathematics and Computers in Simulation 69*, 5-6 (2005), 424–438.

[69] Motsa, S., Sibanda, P., Awad, F., and Shateyi, S. A new spectral-homotopy analysis method for the mhd jeffery–hamel problem. *Computers & Fluids 39*, 7 (2010), 1219–1225.

[70] Nazari, M., Salah, F., Abdul Aziz, Z., and Nilashi, M. Approximate analytic solution for the kdv and burger equations with the homotopy analysis method. *Journal of Applied Mathematics 2012* (2012).

[71] Nield, D., and Kuznetsov, A. Forced convection with laminar pulsating flow in a channel or tube. *International Journal of Thermal Sciences 46*, 6 (2007), 551–560.

[72] Paoli, R., et al. Numerical simulations of shock-shock interactions. *Open Journal of Fluid Dynamics 8*, 04 (2018), 392.

[73] Petropoulou, E. N., and Xenos, M. A. Qualitative, approximate and numerical approaches for the solution of nonlinear differential equations. In *Applications of Nonlinear Analysis*. Springer, 2018, pp. 611–664.

[74] Prasad, P. An introduction to nonlinear hyperbolic waves. In *Nonlinear Hyperbolic Waves in Multidimensions*. Chapman and Hall/CRC, 2001, pp. 17–62.

[75] Rashidi, M., Ganji, D., and Dinarvand, S. Approximate traveling wave solutions of coupled whitham-broer-kaup shallow water equations by homotopy analysis method. *Differential Equations and Nonlinear Mechanics 2008* (2008).

[76] Rowlands, S. Is the arterial pulse a soliton? *Journal of Biological Physics 10*, 4 (1982), 199–200.

[77] Sajid, M., and Hayat, T. Comparison of ham and hpm methods in nonlinear heat conduction and convection equations. *Nonlinear Analysis: Real World Applications 9*, 5 (2008), 2296–2301.

[78] Salas, A., Lozano, W., and Vallejo, L. One and two soliton solutions for the kdv equation via mathematica 7. *International Journal of Applied Mathematics (IJAM) 23* (2010), 1075–1080.

[79] Sarboland, M., and Aminataei, A. On the numerical solution of one-dimensional nonlinear nonhomogeneous burgers' equation. *Journal of Applied Mathematics 2014* (2014).

[80] Schlichting, H., and Gersten, K. *Boundary-layer theory*. Springer, 2016.

[81] Shi, Y., Lawford, P., and Hose, R. Review of zero-d and 1-d models of blood flow in the cardiovascular system. *Biomedical engineering online 10*, 1 (2011), 33.

[82] Strauss, W. A. *Partial differential equations: An introduction*. John Wiley & Sons, 2007.

[83] Sutera, S. P., and Skalak, R. The history of poiseuille's law. *Annual review of fluid mechanics 25*, 1 (1993), 1–20.

[84] Teschl, G. *Ordinary differential equations and dynamical systems*, vol. 140. American Mathematical Soc., 2012.

[85] Trefethen, L. N. Spectral methods in matlab, volume 10 of software, environments, and tools. *Society for Industrial and Applied Mathematics (SIAM), Philadelphia, PA 24* (2000).

[86] Turkyilmazoglu, M. Purely analytic solutions of the compressible boundary layer flow due to a porous rotating disk with heat transfer. *Physics of fluids 21*, 10 (2009), 106104.

[87] Tzirtzilakis, E., Xenos, M., Marinakis, V., and Bountis, T. Interactions and stability of solitary waves in shallow water. *Chaos, Solitons & Fractals 14*, 1 (2002), 87–95.

[88] Vajravelu, K., and Van Gorder, R. *Nonlinear flow phenomena and homotopy analysis*. Springer, 2013.

[89] Versteeg, H. K., and Malalasekera, W. *An introduction to computational fluid dynamics: the finite volume method*. Pearson education, 2007.

[90] Walker, P., Tinkler, L., Royall, B., Skryabin, D., Farrer, I., Ritchie, D., Skolnick, M., and Krizhanovskii, D. Dark solitons in high velocity waveguide polariton fluids. *Physical review letters 119*, 9 (2017), 097403.

[91] Wang, M. Exact solutions for a compound kdv–burgers equation. *Physics Letters A 213*, 5-6 (1996), 279–287.

[92] Wang, S., Tang, X.-y., and Lou, S.-Y. Soliton fission and fusion: Burgers equation and sharma–tasso–olver equation. *Chaos, Solitons & Fractals 21*, 1 (2004), 231–239.

[93] Wang, X.-y. Nerve propagation and wall in liquid crystals. *Physics Letters A 112*, 8 (1985), 402–406.

[94] Wazwaz, A.-M. The tanh method for generalized forms of nonlinear heat conduction and burgers–fisher equations. *Applied Mathematics and Computation 169*, 1 (2005), 321–338.

[95] Wazwaz, A.-M. The tanh–coth and the sech methods for exact solutions of the jaulent–miodek equation. *Physics Letters A 366*, 1-2 (2007), 85–90.

[96] Weiss, J., Tabor, M., and Carnevale, G. The painlevé property for partial differential equations. *Journal of Mathematical Physics 24*, 3 (1983), 522–526.

[97] Whitham, G. B. *Linear and nonlinear waves*, vol. 42. John Wiley & Sons, 2011.

[98] Womersley, J. R. Method for the calculation of velocity, rate of flow and viscous drag in arteries when the pressure gradient is known. *The Journal of physiology 127*, 3 (1955), 553–563.

[99] Xenos, M. A., and Felias, A. C. Nonlinear dynamics of the kdv-b equation and its biomedical applications. In *Nonlinear Analysis, Differential Equations, and Applications*. Springer, 2021, pp. 765–793.

[100] Xenos, M. A., Petropoulou, E. N., Siokis, A., and Mahabaleshwar, U. Solving the nonlinear boundary layer flow equations with pressure gradient and radiation. *Symmetry 12*, 5 (2020), 710.

[101] Xu, D., Lin, Z., Liao, S., and Stiassnie, M. On the steady-state fully resonant progressive waves in water of finite depth. *Journal of Fluid Mechanics 710* (2012), 379–418.